POLITECNICO DI TORINO

Corso di Laurea Magistrale
in Ingegneria Meccanica

Tesi di Laurea Magistrale

Simscape Multibody model of an electric KickScooter

Relatore:

Prof. Alessandro Vigliani

Tutor aziendale:

Ing. Marco Beltrametti

Candidato:

Vincenzo Aquaro

Ottobre 2021

Contents

Acknowledgement

Al termine dei miei studi universitari, è doveroso esprimere la mia gratitudine nei confronti di tutti coloro che hanno contributo al raggiungimento di questo traguardo.
In primis ci tenevo a ringraziare il professor Alessadro Vigliani, nonché relatore di questa tesi, per la disponibilità, la fiducia e l'interesse che ha dimostrato durante l'intero percorso di stesura, ma soprattutto per aver contributo ad arricchire la mia conoscenza professionale, la ringrazio infinitamente.
Un ringraziamento va al mio tutor aziendale Marco Beltrametti, per aver contribuito alla realizzazione di questa tesi, grazie per i consigli e la disponibilità che ha dimostrato.
Un ringraziamento sincero è per i miei genitori e mio fratello, che hanno permesso il raggiungimento di questo importante traguardo, grazie per avermi sostenuto durante l'intero percorso di studi, per avermi trasmesso la giusta carica senza arrendermi mai, per aver gioito dei miei risultati e per essermi stati accanto durante i periodi più difficili, e per non aver mai smesso di credere in me, non finirò mai di dirvi grazie.
Un ringraziamento speciale va alla mia fidanzata Elisabetta, per essermi sempre stata accanto durante i momenti più belli e quelli più difficili, grazie per l'amore che mi hai dimostrato e per avermi sempre supportato trasmettendomi la giusta grinta e la forza per non arrendermi ai primi ostacoli.
Infine, un ringraziamento va a me stesso, per non essermi mai arreso durante il percorso universitario dinanzi alle difficoltà incontrate per aver reagito ed essermi rialzato più forte di prima.

Abstract

This thesis project was carried out in collaboration with TO.TEM , a start-up that designs electric vehicles suitable for urban micro-mobility. In particular, the subject of this project is an electric KickScooter called LYNX, which aims to make the use of such vehicles safer thanks to the presence of three wheels, a large footrest and an anti-collision system based on artificial intelligence. Nowadays, electric scooters are becoming more and more popular in cities as an excellent means of green transport for short journeys. The objective of this thesis is to create a dynamic model of the vehicle in a Virtual Simulation environment, in this case Simscape Multibody. The first part of the paper focuses on the explanation of how the individual subsystems, that make up the vehicle, were realised. The second part describes the measurement chain and the types of experimental tests that were carried out on a prototype. Finally, in the last part, the model is calibrated on the basis of the experimental data acquired and then used to evaluate the benefits of introducing a front suspension.

Chapter 1

Background

Nowadays, the theme of sustainable mobility is one of the most discussed for the environment and our health. In recent decades, all countries have adopted strategies to reduce air pollution, especially in large cities where pollution limits are often exceeded. The transport sector is one of the most revolutionized because it consumes a third of the EU’s final energy. Unlike other sectors, such as energy and industry, where emissions have already decreased since 1990, emissions in transport have increased. This effect is mainly due to the large-scale diffusion of vehicles with internal combustion engines. Over the last decade, EURO regulation has been introduced to reduce pollutant emissions, and this has led car manufacturers to develop technologies and after-treatment systems to fall within the limits imposed by regulations. Nevertheless, to reach the goal of a clean planet, the European Union is promoting the spread of low-emission fuels and zero-emission vehicles.

In this context, a new class of vehicles called micro-vehicles is taking off in big cities because they are easy-to-use, zero-emission means of transport that allows avoiding traffic. Kickscooters, hoverboards, and single-wheelers are all very comfortable ways of traveling the so-called “last-mile”, the last stretch of road that leads to the final destination.

This new way of transport is also spreading thanks to the sharing services whereby e-scooters are made available to use for short-term rentals. This system is becoming more and more popular because it is possible to pick up and drop off the vehicle in a certain service area without the need to reach a specific location for the end of the rental.

The main objective of this work is the creation of a dynamic model of an electric kickscooter called LYNX, designed by the start-up TO.TEM. This vehicle was created after several interviews in which it emerged that a large part of the population does not use this means of transport because considered unsafe. To increase safety and stability LYNX has three wheels, one front and two rear, is equipped with a large footrest platform, and has a collision-alert system with a rear camera and artificial intelligence that warns the driver in case of overtaking by other road users.

All these solutions lead the driver to feel a safer driving sensation thanks to the three wheels, which provide greater stability than two-wheeled vehicles, and to the driver's position, with the feet placed in parallel and not one behind the other as on a traditional kickscooter.
From a sustainability point of view, a circular economy approach is used to decrease the carbon footprint: wood deck, aluminium frame, and batteries are designed to close the product's lifecycle by reintroducing the materials into the supply chain.

Figure 1.1 – LYNX design

1.1 – Human response to vibrations

Since LYNX has been designed to improve driver's feeling of safety and comfort in order to bring a higher user base closer to the use of electric kickscooters, the study of vertical dynamic is of fundamental importance. Unlike conventional vehicles where the vibrations transmitted to the driver can derive from the engine and other mechanical parts, in this case, since the traction is provided by an electric motor, the main source of vibrations is constituted by the irregularities of the road surface. Due to the low maximum speed reached by the vehicle (25 km/h), vibrations generated by the aerodynamic forces can be considered negligible.
Excessive oscillations can represent not only a comfort problem but also a health problem. There are two types of exposures: whole-body vibration (WBD) and local vibration. In the first one, the whole body is in contact with a vibrating source, such as on means of

transport, and suffers its effects, while in the second one the oscillations affect only a specific part of the body, such as hand-arm vibration where vibrating tools are gripped.
Studies on the effect of WBD on human health are very complicated because they are also affected by individual sensitivity parameters. In general, the greatest damage to health occurs when vibrations frequency approaches the natural frequencies of the various parts of the body, and in particular those of the spine, which is the most affected part.
In Italy, the reference norm concerning human exposure to vibration is the UNI ISO 2631-1.

1.1.1 – UNI ISO 2631-1

The UNI ISO 2631-1 defines the criteria for evaluating the vibration disturbance. The legislation does not deal with the health effects caused by oscillations as these depend on numerous biological parameters that vary among individuals.
The frequency range considered is:

- 0.1 Hz to 0.5 Hz for motion sickness;
- 0.5 Hz to 80 HZ for health, comfort, and perception.

The main physical quantity for vibrations measurement is acceleration. Measurement must be taken with a Cartesian reference defined by the regulation, as can be seen in Figure 1.2:

- Z-axis parallel to the spine (vibration along the spine from feet to head)
- Y-axis perpendicular to the femoral axis (vibration along the chest from right to left)
- X-axis orthogonal to the other two axes (vibration across the chest from back to front)

Sensors must be positioned where vibrations enter the body, in the specific case of the kickscooter, where the driver is standing, accelerometers must be placed between the two feet and on the steering wheel.

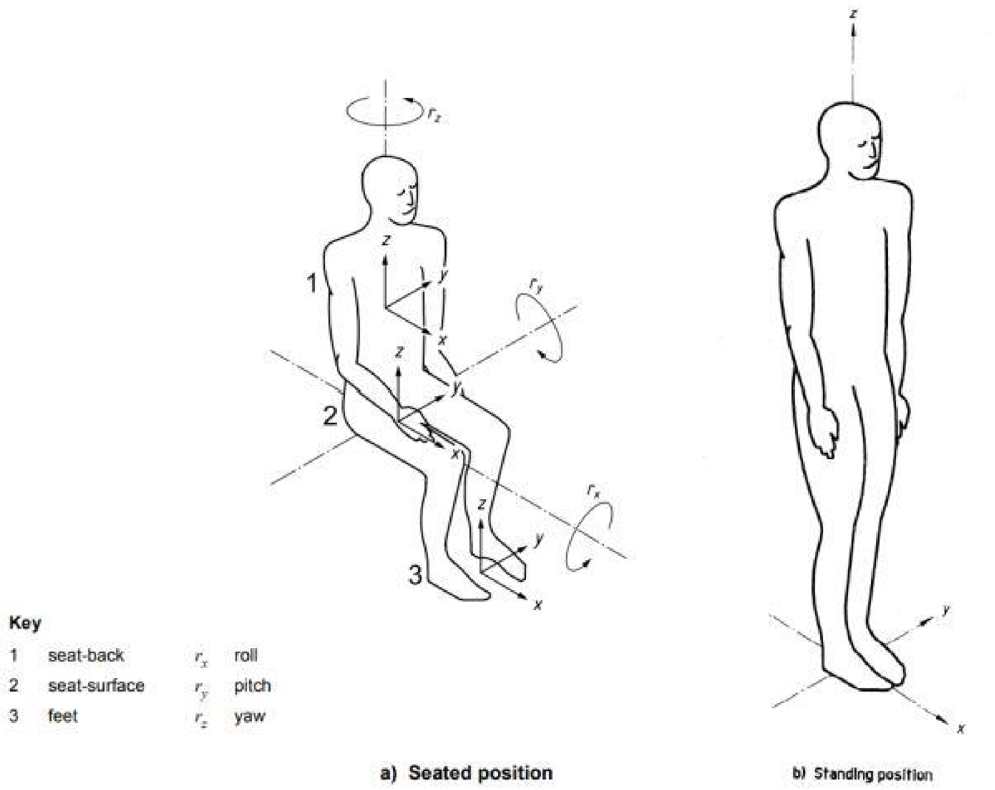

Figure 1.2 – Axis system defined by UNI ISO 2631-1

The evaluation of accelerations according to the ISO 2631-1 standard, requires the frequency-weighted root mean square acceleration on each single axis *l*:

$$a_{wl}(t) = \left[\frac{1}{T} \int_{0}^{T} a_{wl}^{2}(t)dt \right]^{\frac{1}{2}} \tag{1.1}$$

Where:

- $a_{wl}(t)$ is the frequency-weighted acceleration on the *l* axis as a function of time;
- T is the duration of the measurement in seconds.

To find the value of a_{wl} it is necessary to make frequency weighting though the use of weighting curve which take into account human sensitivity to vibration depending on the frequency. These curves are represented in Figure 1.3.

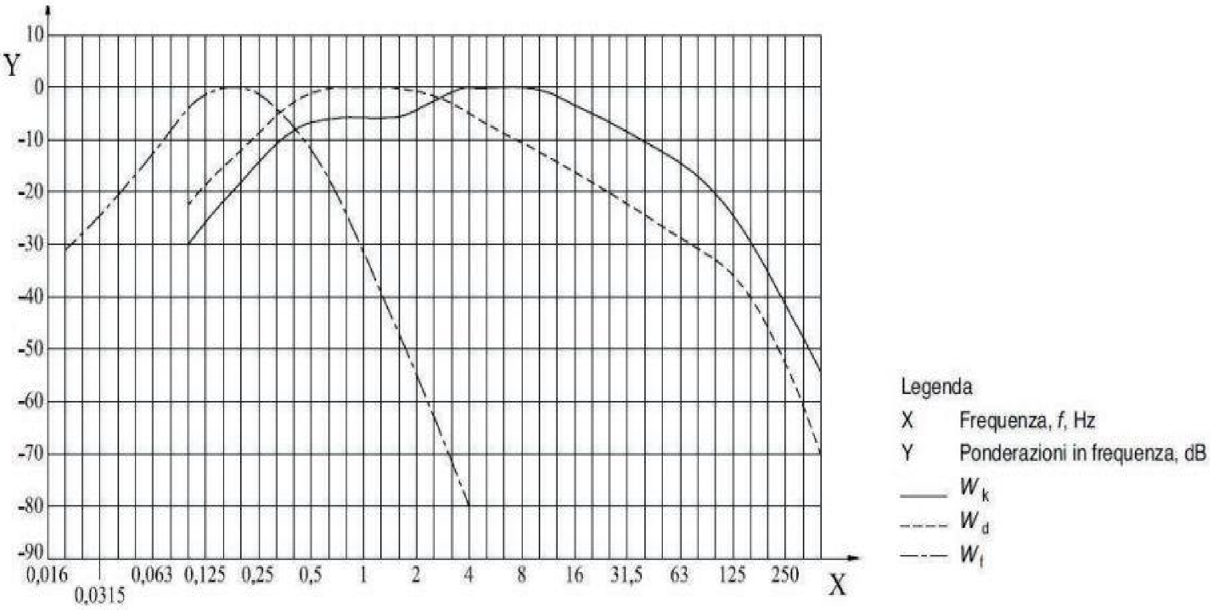

Figure 1.3– Main frequency weighting curves by UNI ISO 2631-1

As shown in figure 1.3, the W_k curve, referred to the vertical axis z, has a maximum between 4 and 10 Hz. This means that the maximum sensitivity of the human body to vertical vibrations, which are responsible for comfort, occurs in this frequency range.

With regard to the other two curves, the W_d , related to oscillations in the horizontal plane, has a maximum in the 1 – 2 Hz interval, while the W_r , responsible for motion sickness, show a maximum around 0.2 Hz.

Chapter 2

LYNX multibody model

The aim of this chapter is to describe the various components of the vehicle and how they were modelled within the simulation software. In the first paragraph, the advantages and phases of virtual prototyping are explained with particular reference to Simscape Multibody, while in the successive ones, all subsystems are analysed, highlighting the simplifications applied and the limitations of use for each of them.

2.1 – Multibody simulation

Multibody simulation (MBS) is a useful tool for conducting kinematic and dynamic analyses of Multibody systems. The latter consists of mechanical parts connected by kinematic constraints (such as joints) or force elements (such as spring-dampers) in order to simulate the relative motion between them.
Over the last few decades, MBS has found an increasingly wide field of application thanks mainly to the increased computing power of PCs and the simplification of the interface of the various programmes, which has made them easy-to-use.
In order for this method to bring benefits, it is necessary that the mechanical system modelled correctly simulates the behaviour of the real one already during the product development phase. If this is the case, the use of virtual prototyping provides several advantages:

- Reduction of error costs: with the use of MBS software, it is possible to detect errors earlier and not during the final stages of product development, where the cost of design changes is higher;
- Reduction of time and costs of testing and tuning;
- Increase the number of tests that can be carried out on the product during the development phase at the same cost and time, reducing the risks due to the reduction of Time-to-Market.

- Reduction life cycle cost: it is possible to bring to the market a product with better quality and reliability that requires few changes over time.

Virtual prototyping can generally be divided into five phases:

1. The first activity is the creation of CAD models of the individual components;
2. CAD models are imported into the simulation software;
3. The individual components are connected with joints and links to create subsystems. The subsystems are then joined together to create the complete system;
4. With the MBS model created, simulations are executed, such as, in the field of road vehicles design, overcoming a road obstacle or performing a certain manoeuvre;
5. The results are then used to optimise specific parameters of the model to reach the desired target.

2.1.1 Simscape Multibody

Simscape multibody is a Matlab extension that enables to perform virtual 3D simulations of mechanical systems such as: robots, vehicles, machinery, and more. All kinds of multibody systems can be created by connecting blocks that represent bodies, joints, force elements, sensors, etc.
The individual parts can be modelled within the software, from fundamental solid shapes, using the appropriate blocks, or through the solid block with which it is possible to import a body made on any CAD saved as a STEP file.
It is possible to integrate physical systems into the model using the Simscape family of products which offers fundamental components in mechanical, electrical, hydraulic, thermal, and other domains.
The software has a mechanical explorer where the model is displayed in a 3D environment from which its structure can be checked. Inside this interface, the results of the simulations are animated and visualized from the desired angle.

One of the main advantages of this extension is that it is fully integrated with Matlab, whereby inputs can be parameterised via a script, and data post-processed, because the model outputs are saved directly in the workspace. In this way, all stages of product development are carried out in a single environment, reducing design time.
A blank model always contains three fundamental blocks without which no simulation can be started:

- The world frame, a unique motionless, orthogonal, right-handed coordinate frame predefined in any mechanical model, the ground of all frame networks;

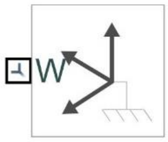

Figure 2.1– World frame block

- The mechanism configurator, a block that defines the simulation parameters of the entire mechanical system. Inside the properties, the value and the direction of the gravity can be defined. As shown in figure 2.2, the gravity value was set to 9,80665 $\frac{m}{s^2}$ in the negative direction of the z-axis;

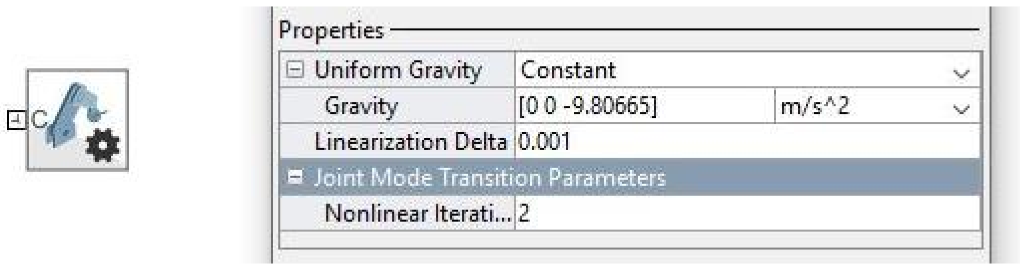

Figure 2.2 – Mechanism configurator block and his properties

- The solver configuration block that defines the solver setting to use for simulation. In the present case, the default parameters were used.

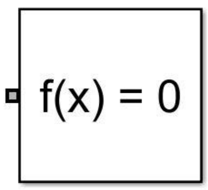

Figure 2.3 – Solver configuration block

2.2 – From CAD to Simscape

This paragraph explains how the Simscape multibody model of the vehicle was realized. The following subsections describe, for each subsystem created, blocks and methodologies used to obtain a dynamic model that is as realistic as possible.
The starting point for Simscape multibody model creation is the CAD of the kickscooter provided by the start-up. During the writing of this paper, the product design was in its last stage, so most of the components used are final.

Figure 2.4 – Starting CAD model

From the initial design, shown in figure 2.4, all those components not considered useful for the purpose of studying vehicle dynamics were removed such as cables, bolts, throttle control, etc. A simplified vehicle was therefore used containing all the main structural parts and those, such as the battery, which contribute significantly to the weight of the e-scooter.

Figure 2.5 – Simplified CAD model

All the bodies were saved as step files and imported into Simscape using the file solid block.

Figure 2.6 – File solid block

This block has a port R that represents a tern of reference axes, associated with the geometry, with which is possible to connect the solid with the others. Inertial parameters and the reference frame can be defined in the properties.
To calculate the mass properties of bodies, two different strategies were adopted:

- For components with a known material, the custom density function was used. With this command, the material density value, saved as a Matlab variable into the start-up file, was entered and the mass, center of mass, moments of inertia, and product of inertia of the body were calculated automatically by the program from the geometry. The list of known materials and their density values is given in Table 2.1.

Material	**Density [kg/m^2]**
C40 steel	7870
6061 aluminium alloy	2710
PA6 plastic	1160

Table 2.1 – Material density

- For components with unknown material, such as tyres, or with internal parts not designed in the imported solid, such as battery and motor, the custom mass function was used. With this command, the mass value, obtained by weighing the actual part (Table 2.2), was entered and the density, center of mass, moments of inertia, and product of inertia of the body were calculated automatically by the program from the geometry. In this case, a simplification was adopted because the battery and the motor were considered as solid bodies with constant density whereas in reality they are made up of a case and internal components and so the center of mass does not correspond to the geometric one. However, this simplification does not lead to great variations in results since the inertial parameters of the entire system are determined by the driver, who represents the main mass.

Component	Mass [Kg]
Front wheel	0.3
Rear wheel	0.2
Battery	3
Motor	3

Table 2.2 – Component weight

For each solid, the reference frame chosen has its origin in the center of mass of the body and orientation equal to the one imported from the CAD file. To do this, in the solid file block properties a new frame, called F, was created.

In figure 2.7, two examples of solid block properties are shown for the frame where the material density is known (left picture) and the motor where the mass is known (right picture).

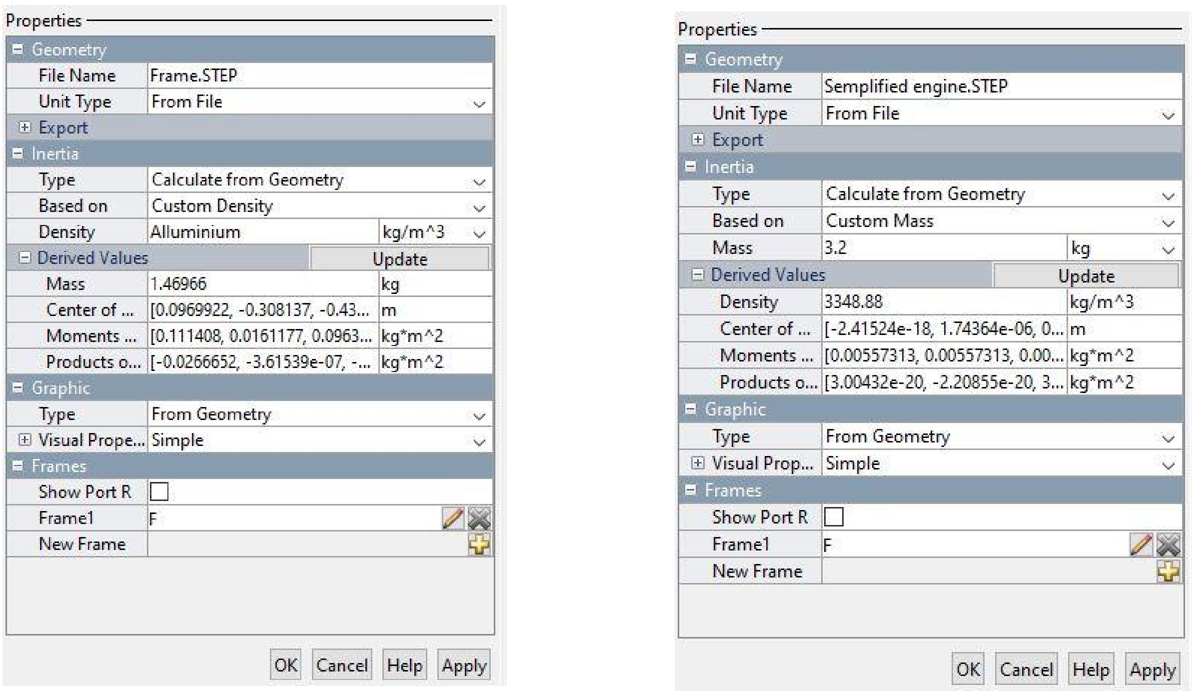

Figure 2.7 – File Solid properties

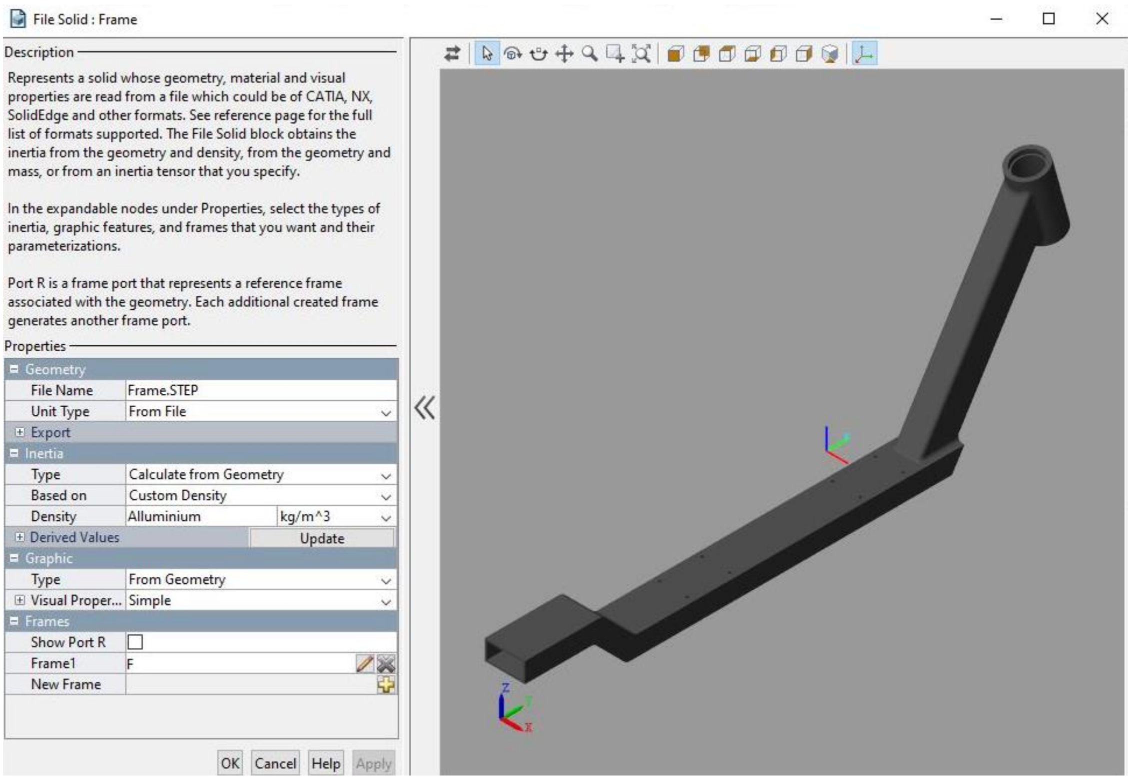

Figure 2.8 – File Solid interface

As shown in figure 2.8, the interface next to the properties displays the imported solid geometry and the tern of reference axes.

To rigidly connect bodies to each other, their reference frames must be joined by a line. To achieve the correct positioning of the parts, the CAD measurement tool was used to measure the distance along the x, y, and z axes between the centres of mass of the components as shown in figure 2.9.

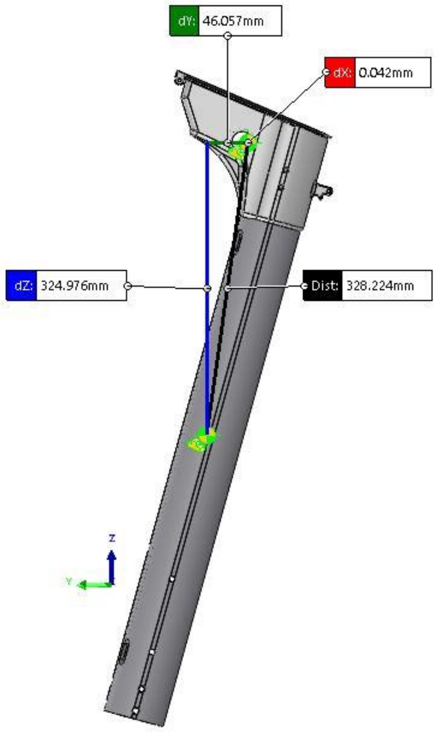

Figure 2.9 – Measuring tool

The data obtained were imported to Simscape using the rigid transform block. This block defines a fixed 3-D rigid transform between B and F that represent the base and follower frames, respectively. In the properties, it is possible to define the rotation and translation of the follower relative to the base in its reference system.

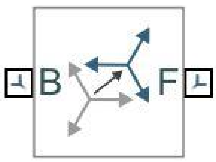

Figure 2.10 – Rigid transform block

By interposing the rigid transformation between the two solid files, the correct distances between the different components were obtained. Using the example given in figure 2.9 the connection between the steering tube and the dashboard in Simscape multibody is made as shown in figure 2.11.

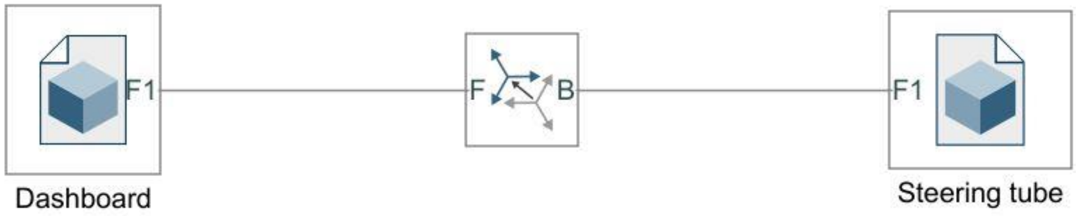

Figure 2.11 – Dashboard and steering tube connection

The two bodies are connected by a continuous line, which means that they can be considered as a single rigid component in which the distances between the points remain constant. This method is a simplification as in reality there are connecting parts, such as screws, that introduce a certain displacement between the parts when subjected to a force. The model consists of ten subsystems that are combined to form the complete vehicle:

- Frame
- Steer
- Front suspension
- Rear suspension
- Front wheel
- Rear left wheel
- Rear right wheel
- Rear fender
- Footrest
- Mannequin

In the following paragraphs, these subsystems will be discussed, except for those such as the steering, the footrest, and the rear fender, which are simply made up of solid bodies connected to each other.

2.3 – Chassis subsystem

The chassis is a square section aluminium profile that represents the backbone of the entire vehicle.

Figure 2.12 – Chassis

For this reason, the chassis subsystem is the central hub of the model to which all the others are linked. As shown in figure 2.17, there are five outputs ports for the connection to the front suspension, the footrest, the steering system, the rear suspension, and the rear fender. In the area highlighted in purple, the connection to the world reference system is made and the degrees of freedom (DOF) assigned to the vehicle are established. The DOFs provided are four:

- Three translational along the x, y, and z axes, using a Cartesian Joint. Through the properties of this block, the initial vertical position of the vehicle was also set to position it in contact with the road at the start of the simulation;

Figure 2.13 – Cartesian Joint block

- One rotational around the pitch axis, using a Revolute Joint. Since this block allows the follower to rotate with respect to the base along the z-axis, there are rigid transformations to make the latter coincide with the pitch axis. Using the properties of the revolute joint, it is possible to log the position signal during the simulation.

Figure 2.14 – Revolute Joint block

This aspect is one of the major limitations of the model because there is no roll or yaw motion. This simplification was adopted because the vehicle is unstable and tended to unbalance and fall during the simulations. Furthermore, since the aim of the paper is to study vertical dynamics and not longitudinal or lateral dynamics, this simplification is considered acceptable.
Still referring to figure 2.17, in the green box there is a transform sensor that measures the time-dependent relationship between follower and base. In the properties of the block, it is possible to select the quantities to be measured, in this case, the position of the vehicle along the three axes, the longitudinal speed in $\frac{km}{h}$ and the vertical acceleration in $\frac{m}{s^2}$.

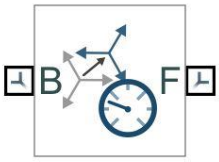

Figure 2.15 – Rigid transform block

Connected to the chassis file solid, there is also an inertia sensor that outputs the mass of the entire system and the position of the center of mass (COM) relative to the frame given as input in the S port of the block.

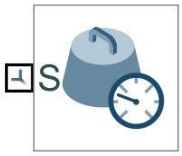

Figure 2.16 – Inertia sensor block

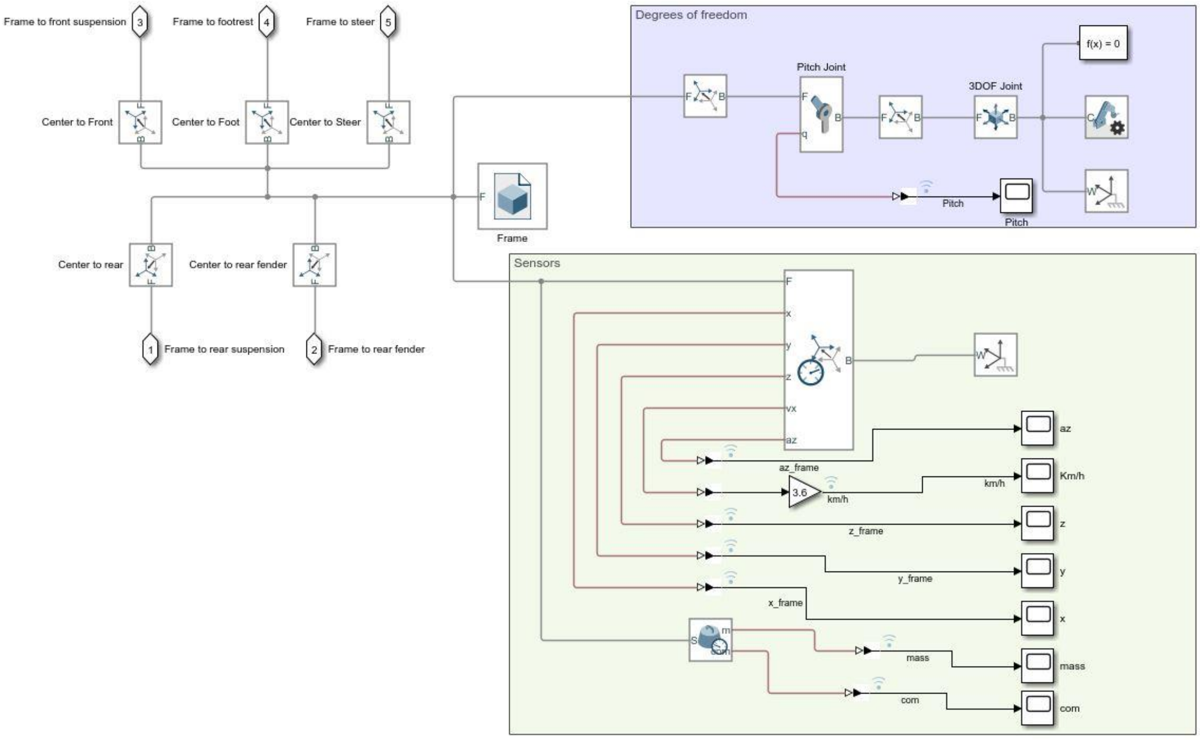

Figure 2.17 – Chassis subsystem

2.4 – Wheels

On a small, urban vehicle like the e-scooter LYNX, different types of wheels can be used, each with its advantages and disadvantages:

- Pneumatic tyres: tyres supported by air pressure. These are the most common used on any vehicle and can be of two different types: with inner tube or tubeless.
    - Tyres with inner tube, common on bicycles and e-scooters, consist of an outer shell inside which there is the tube filled with air. Compared to tubeless ones, they have a worse performance but are easier to repair in the event of a puncture, as it is only necessary to replace the inner tube.
    - Tubeless tyres, common on cars and motorbikes, consist of only the outer tyre that forms an air-tight seal around the rim. Compared to those with inner tubes, they have higher performance and are more resistant to punctures but are also more expensive and difficult to repair.

  In general, the main advantages of pneumatic wheels over the others are more comfortable rides and better shock absorption due to the suspension effect provided by the air, lower rolling resistance and better traction. It is also possible to modify the behaviour of the tyre by adjusting the air pressure. The two main disadvantages are susceptibility to flats and maintenance.

Figure 2.18 – Pneumatic tyre with inner tube

- Solid tyres: tyres not supported by air pressure. The main advantages are that they are immune to flats and require no maintenance. These tyres are mainly used on small vehicles such as e-scooters, bicycles, and golf carts, but also on large vehicles for which a puncture could be a serious problem, such as military vehicles. Their application could also be extended to cars in the future, in fact in 2019 Michelin in collaboration with GM presented UPTIS, shorthand for Unique Puncture-Proof Tire System, an airless tyre concept designed for passenger vehicles. This technology could represent a revolution from an environmental point of view, as it would reduce early tyre changes due to punctures and the production of spare tyres.

  One of the most commonly used structures is the honeycomb design, shown in figure 2.19 for application on scooters. This solution features air pockets in order to reduce the stiffness and improve comfort, which is one of the main disadvantages of solid tyres compared to pneumatic ones.

Figure 2.19 –Honeycomb tyre

- Foam filled tyres: non-pneumatic wheels filled with foam. These represent an excellent compromise between pneumatic and solid wheels in terms of performance and comfort. The insert is a high-strength lightweight material designed to provide pneumatic-like performance by creating simulated pressure, but it has the advantage of solid wheels that it is not subject to punctures. For a city vehicle such as a scooter, this type of wheel can be a solution if no suspension is present. The disadvantage of foam is that being an emerging technology, it has a higher price than a solid wheel and requires more maintenance.

Figure 2.20 – Foam filled tyre

The wheel block is the most complex because inside it the contact with the ground is modelled. The subsystem of the front and rear wheels is the same, with the only difference that on the front there is the vehicle's traction system.

2.4.1 – Sphere to Plane Force

In the first tyre model, the sphere to plane force from Simscape Multibody Contact Force Library was used. In this way, the interaction between the tyre and the road is simplified as a contact between a sphere and a plane. The use of this block is very simple since, as shown in figure 2.21, it is sufficient to connect to the "SphF" port the frame located at the centre of the sphere with any orientation and to the "PlaB" port the frame located at the midpoint of the plane with the z-axis normal to the surface where the force is active. Geometric properties, such as the sphere radius and plane dimensions, the force law, and friction law can be set within the block properties.

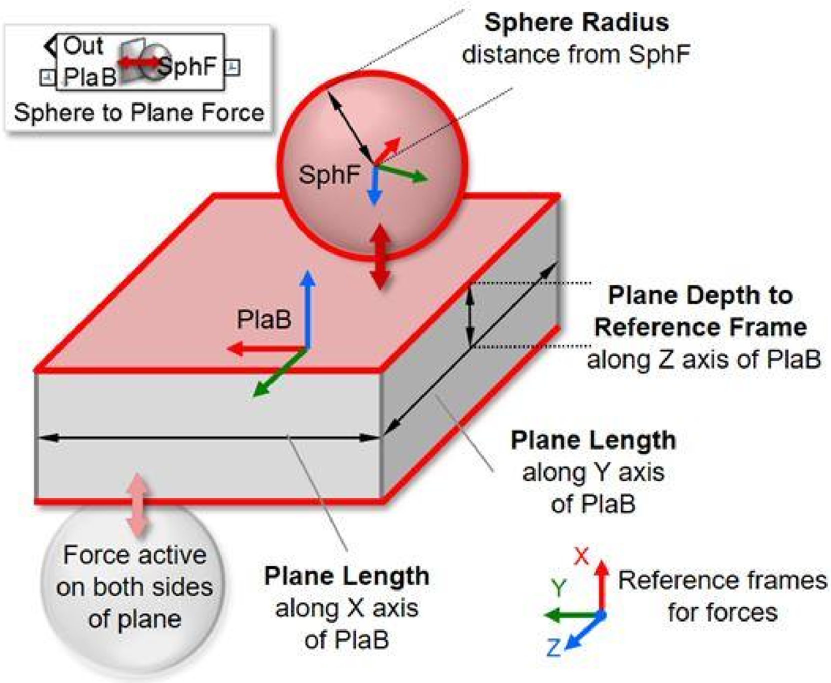

Figure 2.21 – Sphere to Plane Force

With this approach, the modelling of the wheel-ground contact is obtained in a simple way with very good results, but the main limitation, especially for the study of vertical dynamics, is the impossibility of providing a road profile as an input.

2.4.2 – Spatial Contact Force

A generalisation of the sphere to plane modelling is achieved through the use of the spatial contact force block.

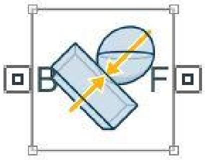

Figure 2.22 – Spatial contact force block

In this case, the contact between wheel and ground is modelled as a contact between two geometries using the penalty method, which allows the bodies to penetrate each other by a small amount. When two solid blocks are connected to the spatial contact force, two forces are applied to both of them as shown in figure 2.23.

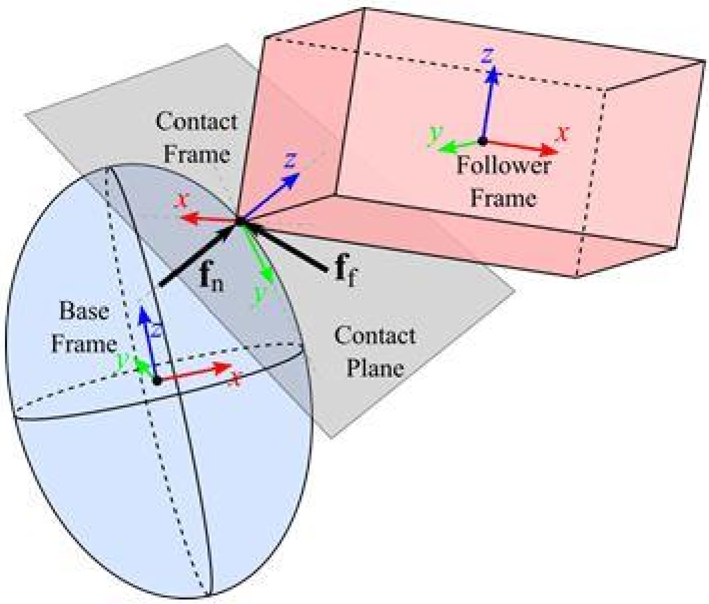

Figure 2.23 – Spatial contact force scheme

where:

- f_n is the normal force perpendicular to the plane of contact which tends to push the bodies apart. This force is calculated using a spring-damper law and therefore depends on the depth and speed of penetration;
- f_f is the friction force which depends on the normal force and the relative speed of the point of contact.

In the block properties (Fig 2.24) it is possible to define:

- Stiffness and damping values;
- The transition region width that defines the penetration value above which the full value of stiffness and damping is applied. In this region the value of the force is gradually increased in order to eliminate discontinuities;
- The coefficient of static and dynamic friction;
- The critical velocity that represents the speed value at which there is a transition from static to dynamic friction.

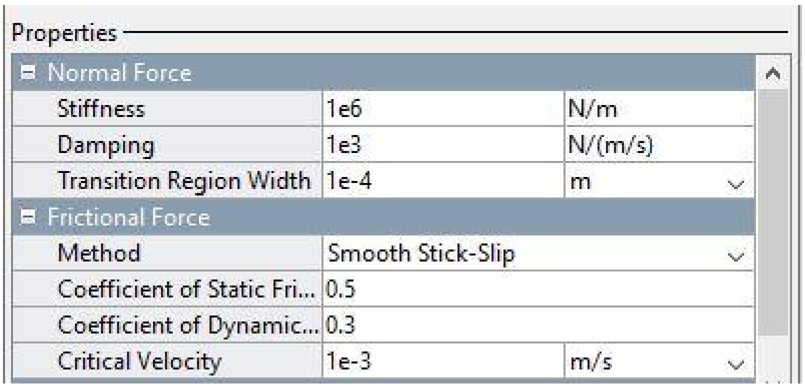

Figure 2.24 – Spatial contact force properties

To use this block, it is necessary to enable the export geometry option in the two solid blocks of which the contact is to be made. In this way, Simscape Multibody creates a convex hull geometry representation that approximates the real geometry of the body, as shown in figure 2.25.

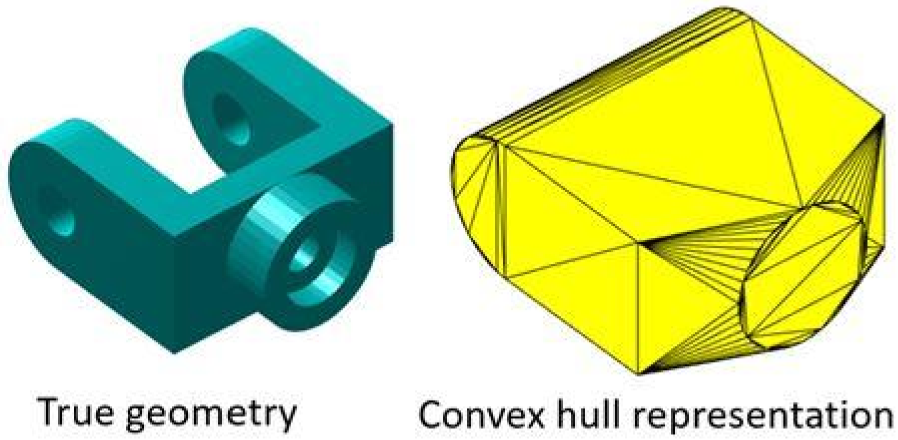

Figure 2.25 – Convex hull representation

With this modelling, it is possible to connect different geometries to the wheel and thus provide a road input to be followed by the vehicle. An example is shown in the figure below where the wheel, represented by a cylindrical geometry, is connected to two solid bricks and another cylindrical solid which simulate a horizontal road with a bump followed by a climb.

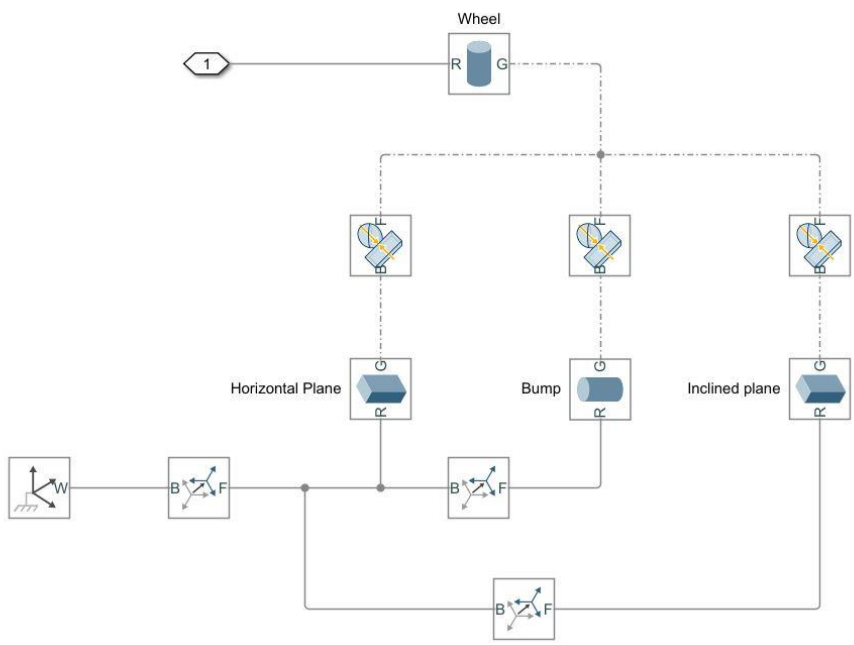

Figure 2.26 – Spatial contact force system example

2.4.3 – CPI tyre model

In this model, the Contact Point Interface (CPI) tyre model from Mfeval toolbox was used. The CPI block, shown in figure 2.27, evaluates the Magic Formula in the contact point between the tyre and the road.

Figure 2.27 – CPI tyre model block

The coordinate system used in all calculations is the W-axis system defined by the TYDEX group:

- The XW-axis is obtained from the intersection between the central plane of the wheel and the surface of the track;
- The YW axis is obtained from the projection of the rotation axis on the ground;
- The ZW-axis is normal to the ground and points upwards.

The origin of the coordinate system is called "wheel intersection point". All the angles (α, γ, ω) shown in picture 2.28 are positive, and force and moment represented act from tyre to rim.

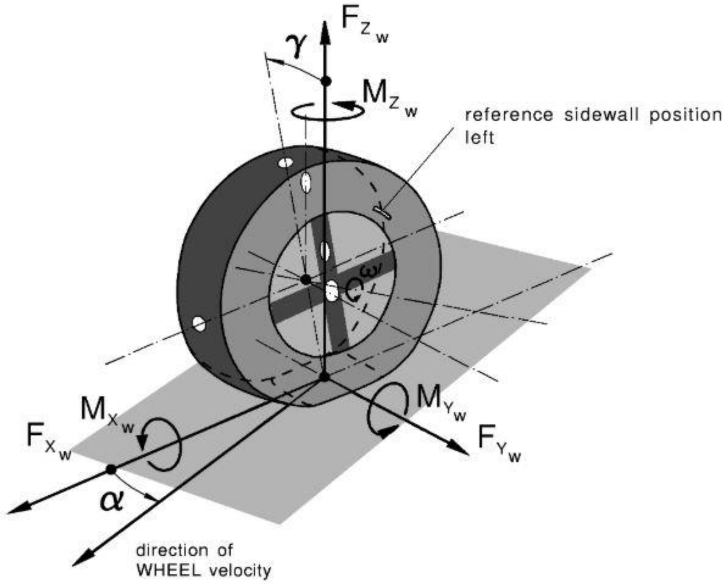

Figure 2.28 – CPI tyre model axis

Eight inputs are required for the model to work:

- Omega (ω) in $\left[\frac{rad}{s}\right]$ is the wheel rotational speed about its spin axis;
- V_x in $\left[\frac{m}{s}\right]$ is the speed of the wheel centre along its longitudinal axis;
- V_{sy} in $\left[\frac{m}{s}\right]$ is the lateral wheel slip speed in the contact point;
- Camber in [rad] defines the inclination of the wheel centreline in relation to the vertical to the ground;
- Psi_dot ($\dot{\Psi}$) in $\left[\frac{rad}{s}\right]$ is the tyre yaw speed about the road normal
- F_z in [N] is the tyre normal load in the contact point;
- muRoad [-] is a double input that indicates longitudinal and lateral friction coefficient between the tire and the road;
- MF-Tyre property file (.Tir) that contains all the tyre properties.

The outputs from the block are:

- F_x in [N] is the tyre longitudinal force
- F_y in [N] is the tyre lateral force

- F_z in [N] is the tyre vertical force which is bypassed from the input
- M_x in $\left[\frac{N}{m}\right]$ is the tyre overturning moment
- M_y in $\left[\frac{N}{m}\right]$ is the tyre rolling resistance moment
- M_z in $\left[\frac{N}{m}\right]$ is the tyre self-aligning moment
- Varinf contains various information that can be tracked using a bus selector block.

In order to integrate the CPI tyre block into the model and adapt it to the purpose of this study, simplifications were adopted. From figure 2.29, it can be seen that:

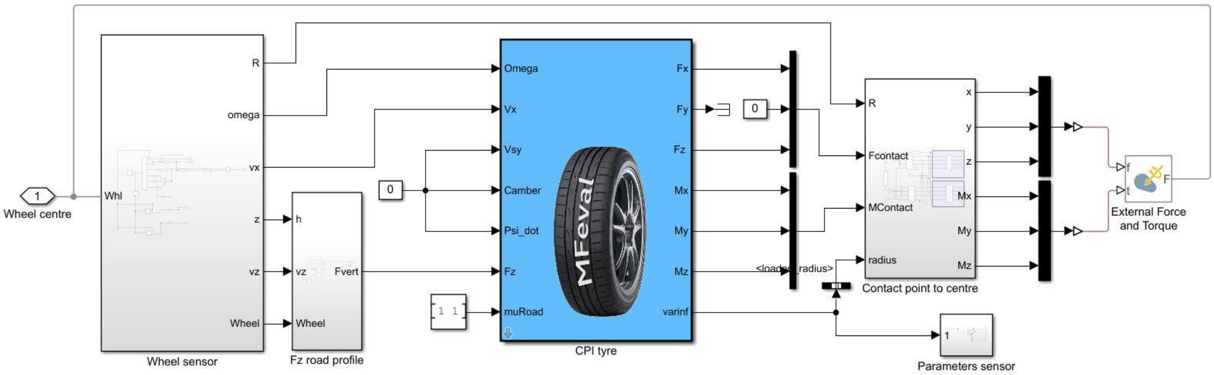

Figure 2.29 – CPI tyre model system

- The value of camber was set to zero because the vehicle's wheels are perpendicular to the ground;
- The values of V_{sy}, and $\dot{\Psi}$ were set to zero because only movement along the longitudinal axis was considered in the simulations carried out;
- The ω and V_x values were obtained through the use of a transform sensor positioned in the centre of the wheel inside the subsystem "Wheel sensor";
- The output F_y was set to 0 because, due to the particular configuration of the vehicle, the front wheel is in the central position, while in the block properties it is only possible to select the left or right side. For the rear, on the other hand, the F_y port was used because, since there are two wheels, the lateral forces calculated were opposite and the resultant null.

The value of the vertical force was calculated in the "F_z road profile" subsystem. The CPI model, in fact, does not describe the vertical dynamics of the wheel since the input F_z is directly bypassed in the output. In figure 2.31, in which the subsystem used for the calculation of the vertical force is fully reported, it can be noted that the wheel was assumed similar to a spring-damper system. In the first part (blue area) the tyre deflection is calculated by subtracting the tyre radius and the road height from the hub height.
To define a given road profile, a 1-D lookup table with the position along x and z of some known points was used.

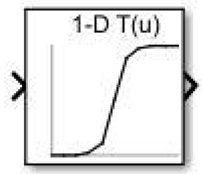

Figure 2.30 – 1-D lookup table

The height of the road, along the z-axis, is calculated by interpolation of table values, based on the position along the x-axis of the wheel which is provided as input to the block. In this way, it is possible to transform the road profile as a function of space, into a time-dependent input based on the speed of the vehicle.
The tire deflection calculated is multiplied by the wheel stiffness (green area) to obtain the spring force:

$$F_k = -kx \tag{2.1}$$

In the last part (purple area), the damping force is calculated:

$$F_d = -bv_z \tag{2.2}$$

The two forces are then added together to form the vertical force acting on the tyre which is given as input to the block CPI.

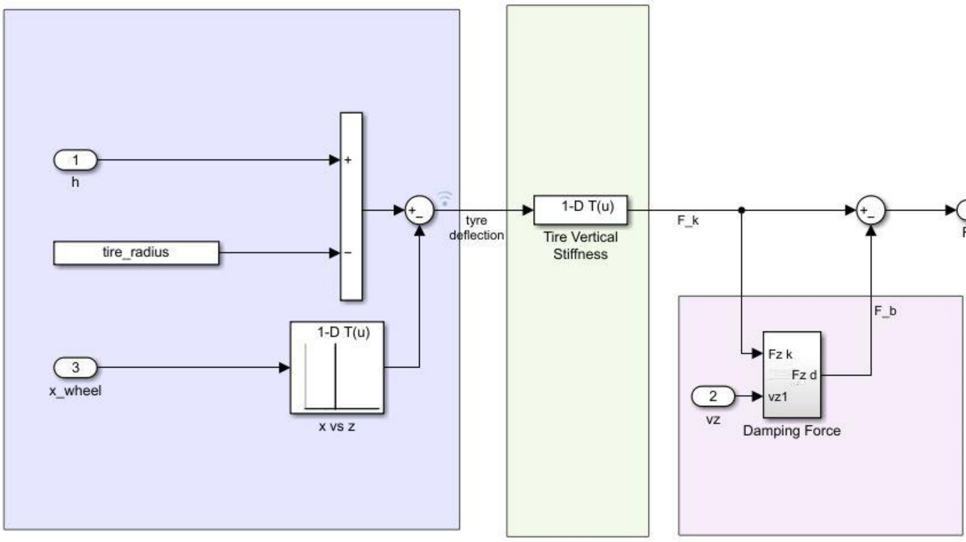

Figure 2.31 – Tyre vertical dynamic

The .tir file used in this application contains the correct geometric parameters of the wheels used on the kickscooter, but all the other coefficients for the calculation of the Pajceka formula are standard for automotive applications. This means that the dynamic longitudinal and lateral performances are not the real ones of the vehicle, due to the lack of tyre data. A future development of the model could involve substituting the correct parameters by performing a fitting process based on real tests.

After calculating the forces and moments with the CPI block at the point of contact, these are transported to the centre of the wheel, by calculating the transport moments for the forces, using the loaded radius information, and transformed from fixed to rotating. Forces and moments are given as input to the external force and torque block which applies them to the frame to which it is connected in port F, in this case to the wheel centre.

In order to provide propulsion to the vehicle, the electric motor was not modelled but the speed value was provided directly as input to the rotational block through the model described below.

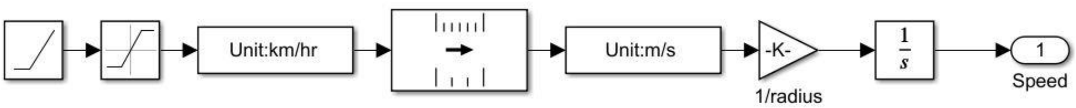

Figure 2.32 – Propulsion system

As can be seen in figure 2.32, the speed increases linearly until it reaches a maximum value due to the saturation lock. The speed is then converted from km/h to m/s and divided by the wheel radius to calculate the angular velocity. The angular velocity is integrated to calculate the angle required to achieve the desired speed and this value is provided as input to the rotational joint.

2.5 – Rear truck subsystem

On the rear axle of the e-scooter, a truck used on skateboards is mounted. A skateboard truck is a T-shaped mechanical device used to link the tilt of the table to the rotation of the wheel axle. Its main parts are:

- The baseplate, a metal component directly screwed to the chassis on which the pivot cup and kingpin are located;
- The hanger, a component directly connected to the wheels through the axle and to the baseplate through the kingpin. The vertical end of the hanger has a pin that engages directly with the pivot cup on the baseplate and represents the fulcrum around which the entire component rotates;
- The kingpin, the connecting bolt between the baseplate and the hanger. By adjusting the tightening torque, it is possible to change the hardness of the bushings and quickly modify the cornering behaviour of the vehicle. This operation is similar to increasing the spring preload in a shock absorber;
- Bushings, polyurethane parts positioned on the kingpin between the baseplate and the hanger that oppose the rotation of the truck around the pivot axis. Their shape, size, degree of hardness and the quality of the polyurethane can greatly vary the feel of the truck when cornering. Harder bushes lead to a less reactive but more stable board at speed, while softer rubbers increase manoeuvrability at the expense of stability. The choice of hardness depends on many factors, including the weight of the driver, the intended use of the truck and also subjective tastes.

When the board is tilted, the hanger makes a rotation around an ideal axis called the pivot axis. Since the latter is oblique, this leads to a rotation of the wheel axle along the ground normal. In this way, steering is realised. One of the most characteristic truck parameters is the lean/turn ratio (LTR), which depends on the inclination angle of the pivot axis and determines by how much the deck must be tilted in order to steer the vehicle by a certain angle. The greater the pivot axis tilt, the smaller the inclination required to turn the vehicle by a certain angle.

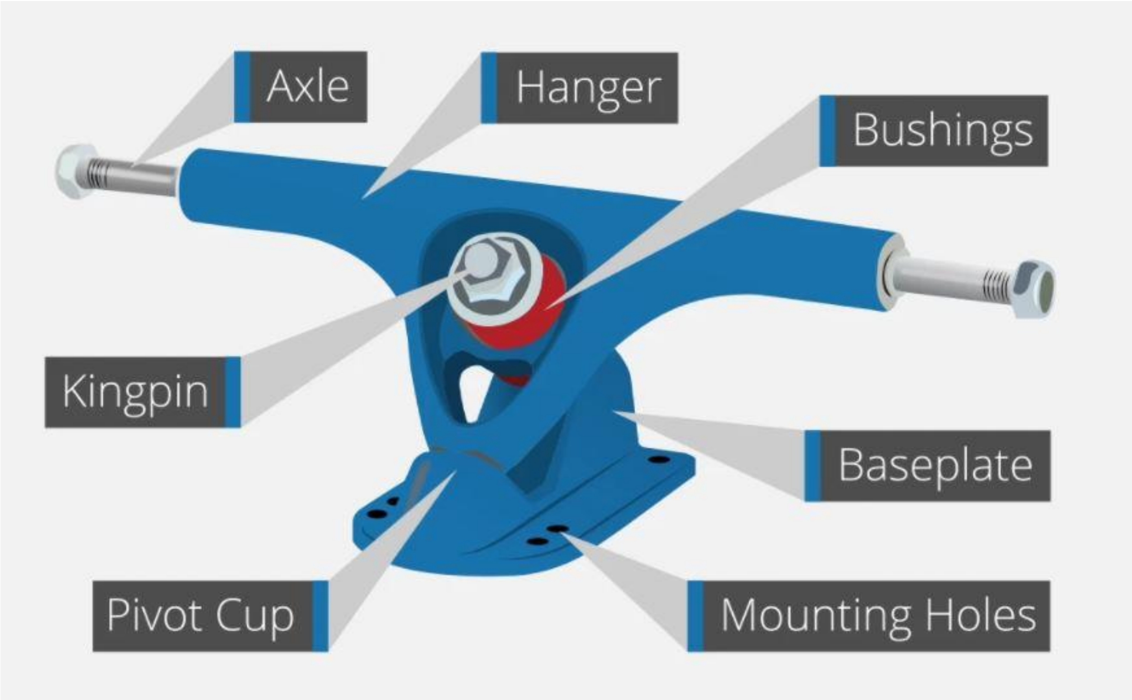

Figure 2.33 – Rear truck scheme

A 45-degree truck produced by Seismic, shown in figure 2.34, is used for LYNX.

Figure 2.34 – Seismic 45-degree rear truck

Since the 3D CAD of the part was not provided by the manufacturer, a simplified spring truck was created using Solidworks. The operating principle of a spring truck is similar to the one with bushings. It consists of a hanger that rotates around a baseplate, but in this case, the springs oppose the movement. A truck available on the market suitable for application on electric skateboards was used as a reference (Fig. 2.35).

Figure 2.35 – Trampa spring rear truck

To have an inclined pivot axis, the truck must be mounted on a sloping surface, or an angular shim must be placed on the baseplate. The component designed, shown in figure 2.36, has the same geometric parameters of the truck actually used on LYNX such as axle height and width.

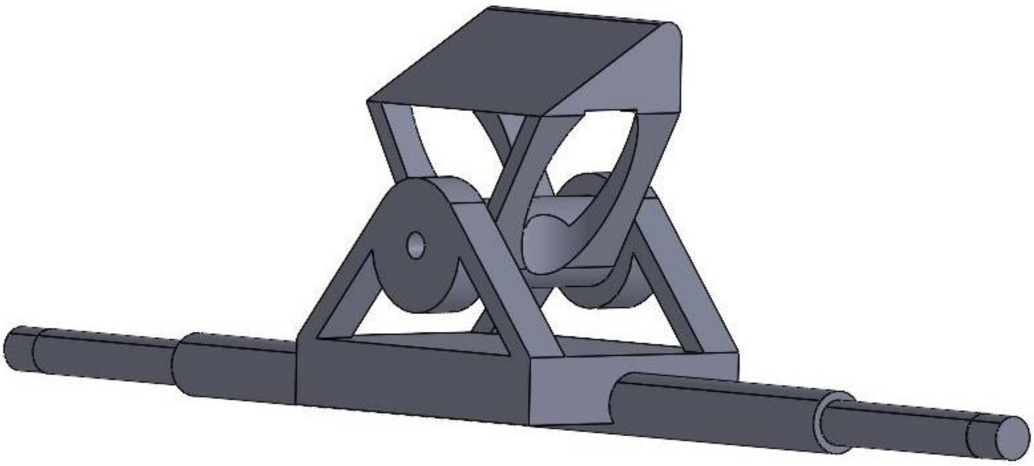

Figure 2.36 – Rear truck side view

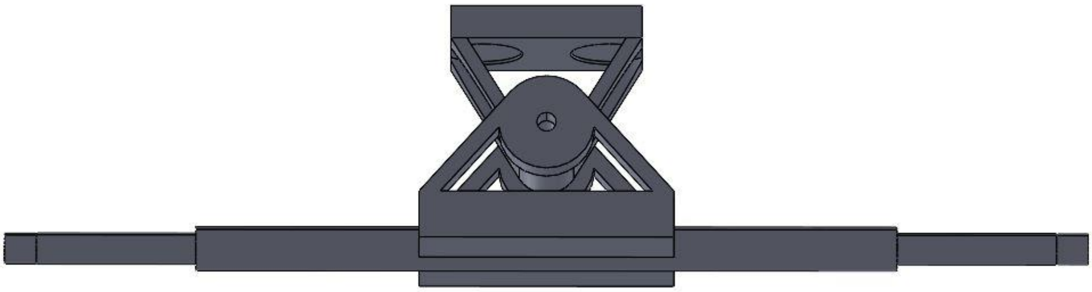

Figure 2.37 – Rear truck bottom view

The baseplate has two circular recesses for the housing of the springs. The connection surface with the frame is tilted by 45 degrees to obtain a pivot axis inclined at the same angle. The complete Simscape subsystem is shown in figure 2.38.

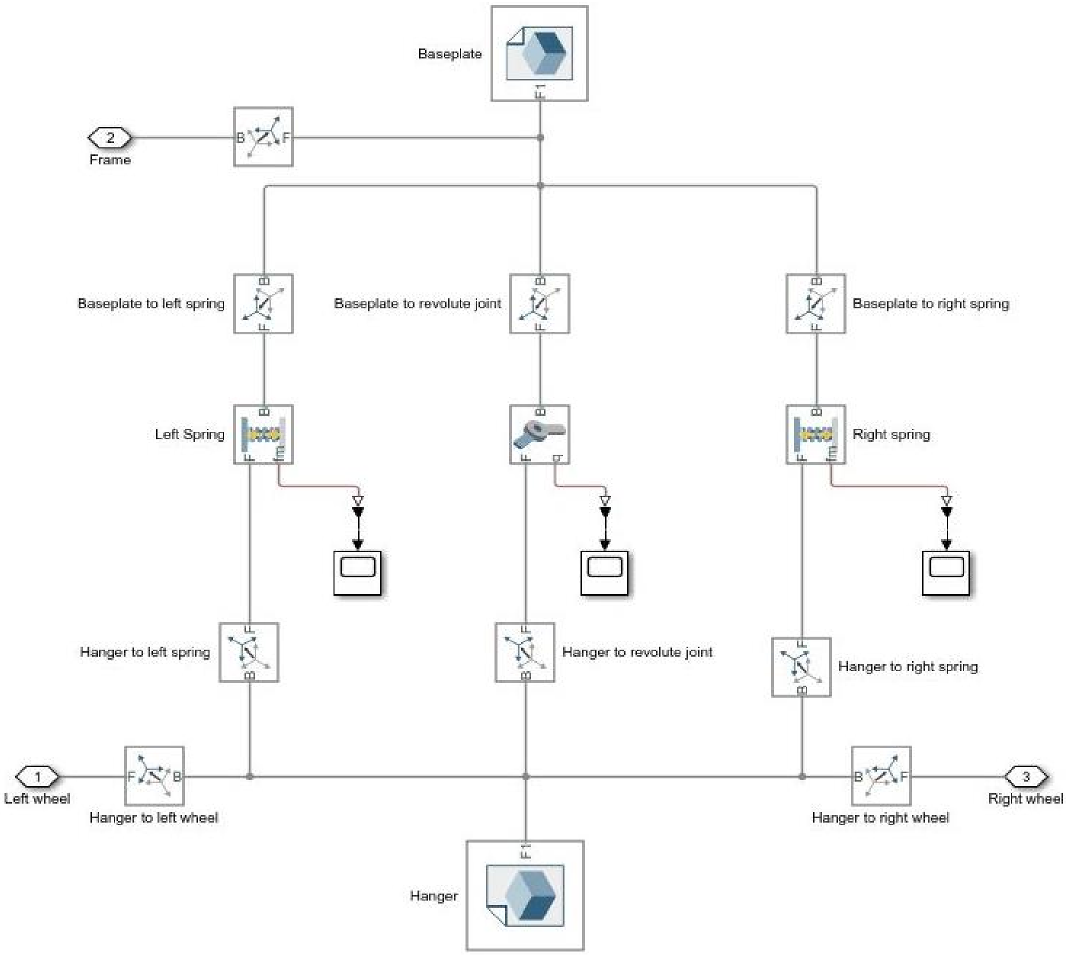

Figure 2.38 – Rear truck system

Inside the subsystem there are two solid rows representing the baseplate and the hanger. These two components are connected in the central part by a rotational joint and at its sides there are two spring damper blocks.

Figure 2.39 – Spring and damper force block

This block represents a linear spring and damper force pair acting between the base and follower frame origin along the line segment connecting the two. The two forces have equal magnitude but opposite directions. The magnitude of the spring force depends on the deformation of the spring with respect to its natural length, while the magnitude of the damping force depends on the relative velocity between the two connected frames.
In the block properties, it is possible to define the natural length of the spring, with which a certain preload can be set and the stiffness and damping values.
The component displayed in the Simscape mechanics explorer is shown in figure 2.40.

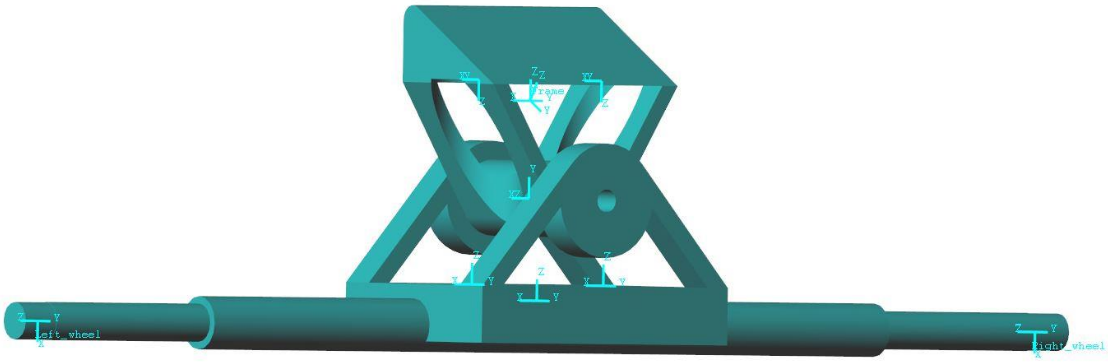

Figure 2.40 – Connection point rear truck mechanics explorer

2.6 – Front suspension subsystem

On the LYNX e-scooter it is possible to install a front suspension, shown in figure 2.41.

Figure 2.41 – Front suspension

This component was designed as two bodies, one solid and the other hollow, both with a hexagonal base to prevent rotation, which slide inside each other, between which a low-friction material is placed. To oppose this movement there is a spring and a rubber bellows which offers a small damping capacity. As can be seen from figure 2.42, which shows a sectional view of the component, there are steps on the two bodies that define the suspension stroke.

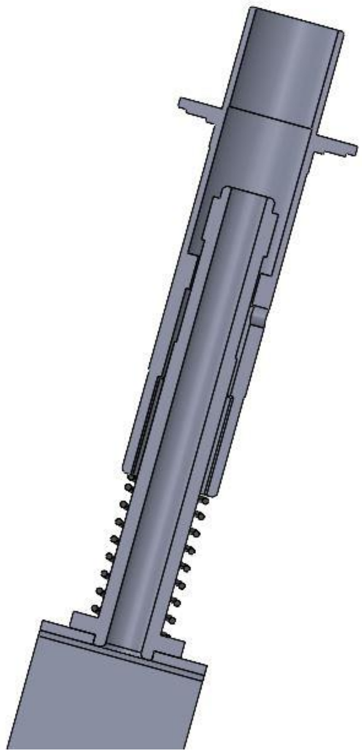

Figure 2.42 – Front suspension section

To simplify the modelling in Simscape, two cylinders were created in the CAD, one solid and one hollow, which slide inside each other.

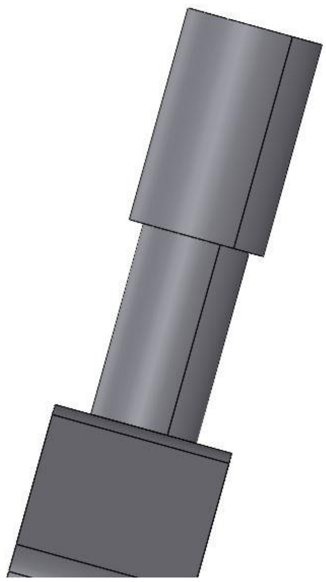

Figure 2.43 – Simplified front suspension

These two solid bodies were connected by a prismatic joint that does not allow rotation but only translation along the z-axis. To design the suspension, it was decided to use a Simscape model shown in figure 2.44.

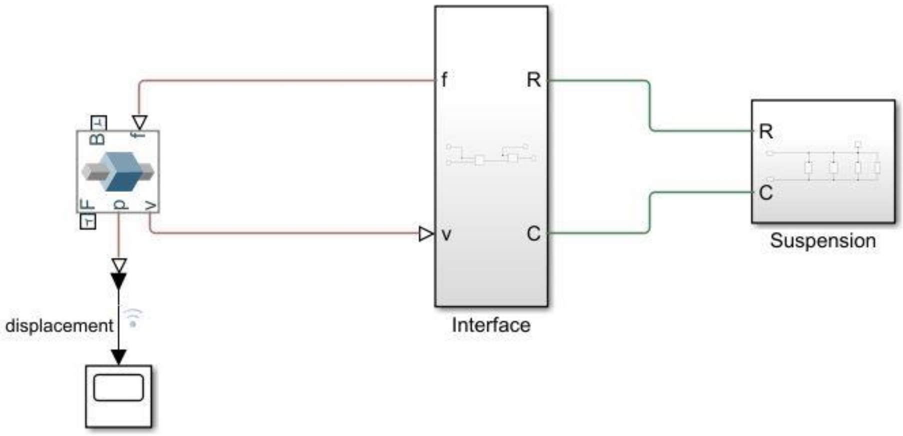

Figure 2.44 – Front suspension system

In the properties of the prismatic joint, the speed option was activated in the sensing tab. The speed information is transmitted to the interface subsystem. Within this system, displayed in figure 2.45, there is a block called "Ideal Translational Velocity Source" which generates a speed difference at its terminals R and C representing conservative mechanical translational conserving ports.

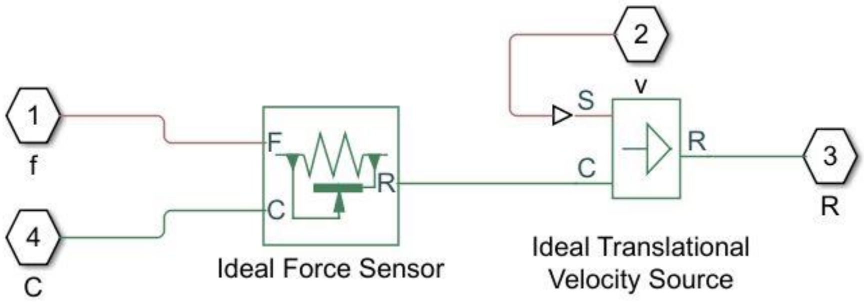

Figure 2.45 – Interface subsystem

Between the R and C terminals, in the suspension subsystem, there are a series of blocks in parallel that simulate the behaviour of a suspension:

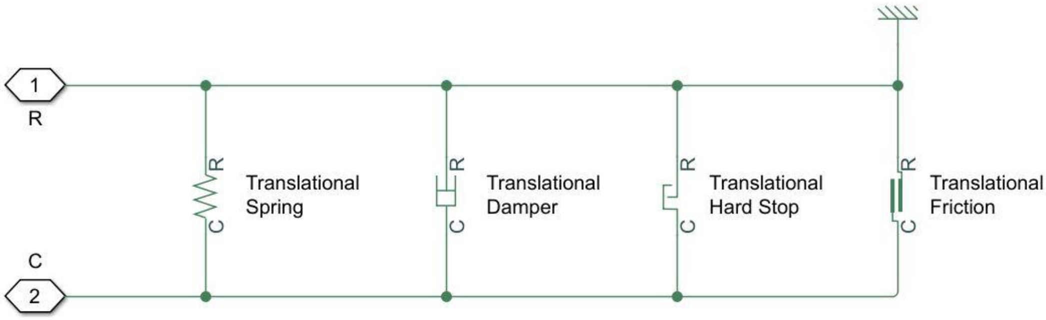

Figure 2.46 – Suspension Subsystem

- **Translational spring** representing an ideal linear spring that follows the equations below:

$$F = K\,x \tag{2.3}$$

$$x = x_{init} + x_R - x_C \tag{2.4}$$

$$v = \frac{dx}{dt} \tag{2.5}$$

In the block properties it is possible to set the initial speed, force, and deformation;

- **Translational damper** representing a linear viscous damper described by the following equation:

$$F = D\,v \tag{2.6}$$

Where:

- v is the relative velocity $v = v_R - v_C$;
- D is the damping coefficient.

In the case of a non-linear damper, it is possible to replace this block with a non-linear translational damper, which allows the insertion of a force/speed curve that can be symmetrical or asymmetrical with respect to the zero-speed point, in order to distinguish expansion and compression damping;

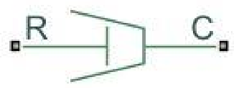

Figure 2.47 – Non-linear translational damper

- **Translational hard stop** is a block that restricts the translational motion of a body between an upper and lower limit. The two boundaries are modelled using a spring-damper system, with the spring opposing penetration between the body and the stop, while the damper takes into account non-elastic effects that cause energy dissipation.

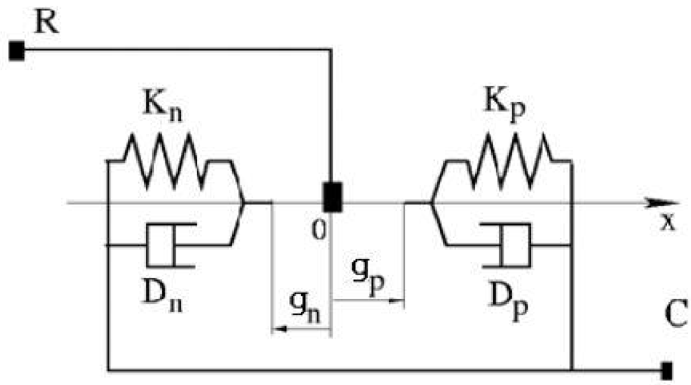

Figure 2.48 – Translational hard stop scheme

Where:

- K_n and K_p are the lower and upper boundary stiffnesses;
- D_n and D_p are the damping coefficients at the lower and upper boundaries;
- g_n and g_d are the initial distances from the lower and upper boundaries.

In the block properties it is possible to select different modes of operation including "Full stiffness and damping applied at bounds, undamped rebound", in which the equations governing the block are:

$$F = \begin{cases} K_p \cdot \left(x - g_p\right) + D_p \cdot v \cdot ge(v,0) & for\ x > g_p \\ 0 & for\ g_n < x < g_p \\ K_n \cdot (x - g_n) + D_n \cdot v \cdot le(v,0) & for\ x > g_p \end{cases} \quad (2.7)$$

The functions ge and le stand for larger or equal and smaller or equal, respectively. Among the other modes that can be selected are the mode with rebound damping and the mode with stiffness and damping that increase linearly until reaching the maximum value at the boundaries;

- **Translational friction** is a block that models the frictional force resulting from contact between two bodies. This block calculates the friction force taking into account the Coulomb, Stribeck and viscous contributions as can be seen from the graph shown in figure 2.49.

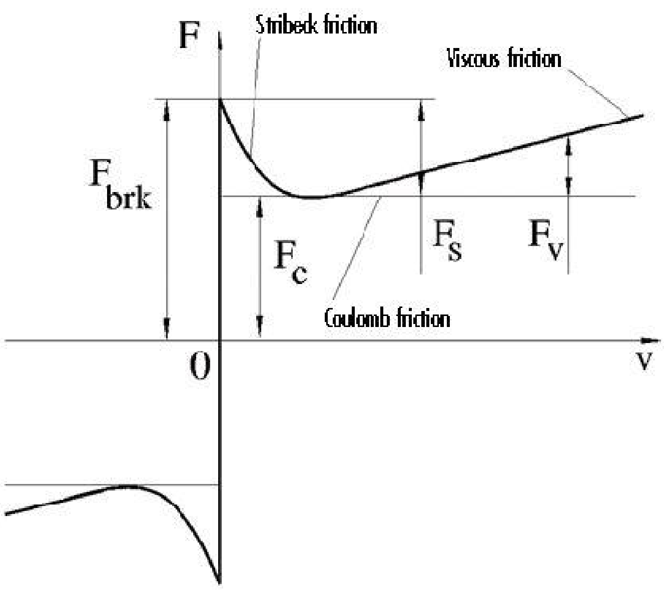

Figure 2.49 – Friction force as a function of speed

The Coulomb friction force is described by the following equation:

$$F_c = \mu F_N \tag{2.8}$$

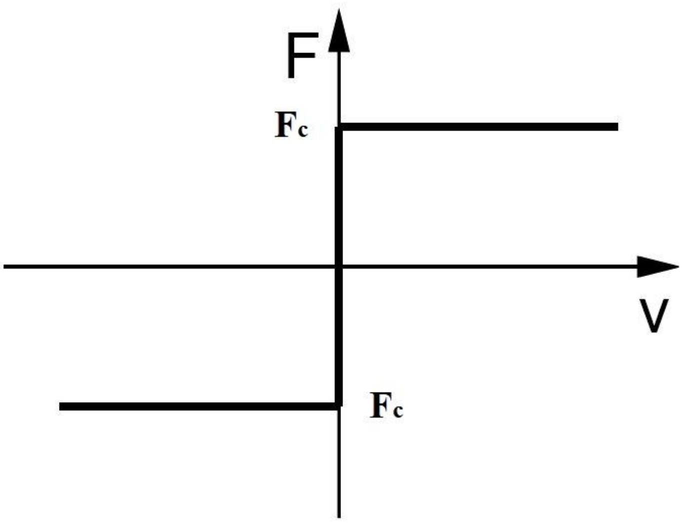

Figure 2.50 – Coulomb friction force

Where μ is is the dynamic friction coefficient and F_N is the normal force. As can be seen from the graph above, the Coulomb force is constant for any value of velocity, while for $v = 0$ it is not defined as it can take on any value in the range F_c / $-F_c$.

The viscous friction force is described by the equation:

$$F_c = k_v v \tag{2.9}$$

Where k_v is the viscous friction coefficient. From formula 2.9, it can be seen that this frictional force contribution increases with increasing speed.

Stribeck friction is a negative slope effect that occurs from static to Coulomb friction. This effect is described by the equation:

$$F_{st} = \sqrt{2}\,(F_{brk} - F_C)e^{-\left(\frac{v}{v_{st}}\right)^2} \tag{2.10}$$

Where F_{brk} is the sum of Coulomb and Stribeck friction force and v_{st} is the Stribeck velocity threshold defined as $v_{st} = v_{brk}\,\sqrt{2}$.
The block estimates the friction force by taking these three force components into account according to the equation:

$$F = \sqrt{2}(F_{brk} - F_C)e^{-\left(\frac{v}{v_{st}}\right)^2} \cdot \frac{v}{v_{st}} + F_c \tanh\left(\frac{v}{v_{Coul}}\right) + k_v\, v \tag{2.11}$$

Where v_{Coul} is the Coulomb velocity threshold defined as $v_{Coul} = \frac{v_{brk}}{10}$. The hyperbolic function used in the Coulomb portion allows to obtain a continuous function around zero with the force immediately reaching its maximum value at very low speeds.
Once the friction force is evaluated, the value is transmitted to the "Ideal Force Sensor block", located in the interface subsystem (Fig. 2.45), which converts the variable passing through the sensor into a control signal. This signal is given as input to the prismatic joint, simulating the effect of suspension.

2.7 - Mannequin subsystem

To simulate the presence of the driver of the vehicle, a dummy was used. This subsystem is fundamental for the execution of reliable simulations, as it represents the major component in weight of the vehicle-driver system. The dummy used has a height of 1.80 m and a mass of 80 kg. The assembly consists of 14 bodies, connected together by rotational and spherical joints.

Bone Names	Mass (% of body weight)	Mass [kg]
Head + Neck	6.94	5.55
Trunk	43.46	34.77
Arm (x 2) - Upper arm - Forearm + Hand	4.94 2.71 2.23	3.95 2.17 1.78
Leg (x 2) -Thighs -Shanks + Feet	19.86 14.16 5.70	15.89 11.33 4.56
Total	100	80

Table 2.3– Body segment mass

To import the dummy into the Simscape environment, the “smimport” function was used. This command automatically generates a Simscape Multibody model from the CAD. In addition to the model, “smimport” also generates a parameter data file, a structure array populated with MATLAB variables in which the block parameters of the imported system are set. In this case, as shown in the complete system in figure 2.51, the initialisation file contains:

- The position of the bodies with respect to a predefined Cartesian reference system;
- The inertial properties of bodies;
- The positions and angles of rotational and spheroidal joints;

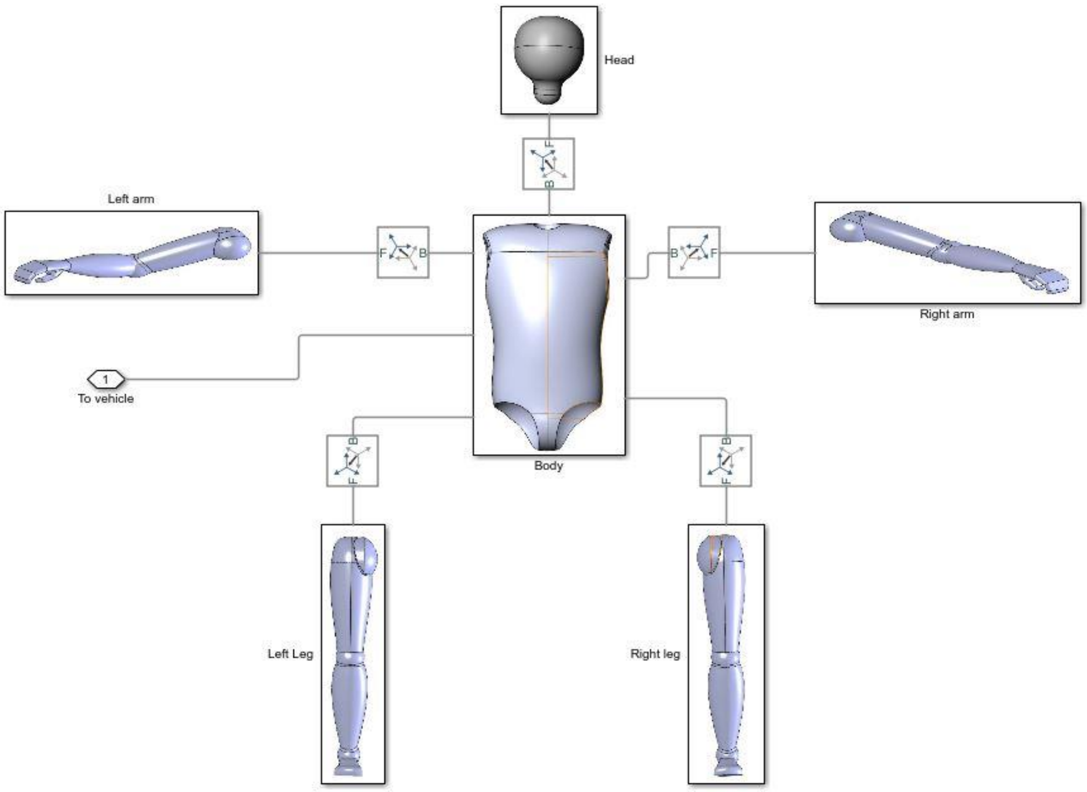

Figure 2.51 – Mannequin subsystem

To reproduce the same posture as the driver, the position of individual limbs was manually modified on the CAD and then the assembly was imported into Simscape. In order to avoid movement during the vehicle's motion, the joints were replaced with rigid links using the same positions and angles as in the parameter data file. In this way, a completely rigid human body model was obtained and placed on the vehicle.

This subsystem, however, represents one of the major simplifications of the model since in reality the driver, while riding the vehicle, moves by varying the centre of mass of the system and exchanges forces with it both on the footrest and the handlebars. In the model, as explained, the dummy has a fixed position and does not exchange forces with the vehicle.

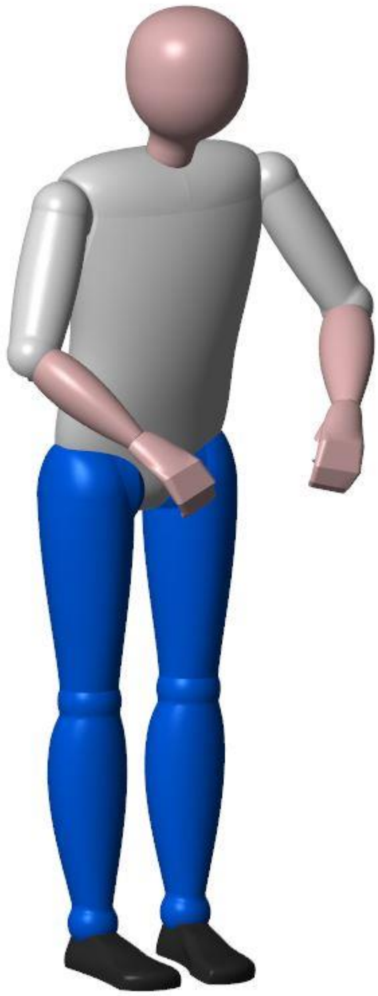

Figure 2.52 – Mannequin subsystem Mechanics Explorer

2.8 – Complete model

All the subsystems shown in the previous paragraphs were joined together to create the complete vehicle and driver model, as shown in figure 2.53. Inside the wheel subsystem, there are all the road wheel contact models discussed in paragraph 2.4, and it is possible to select which of them to use for the simulations.

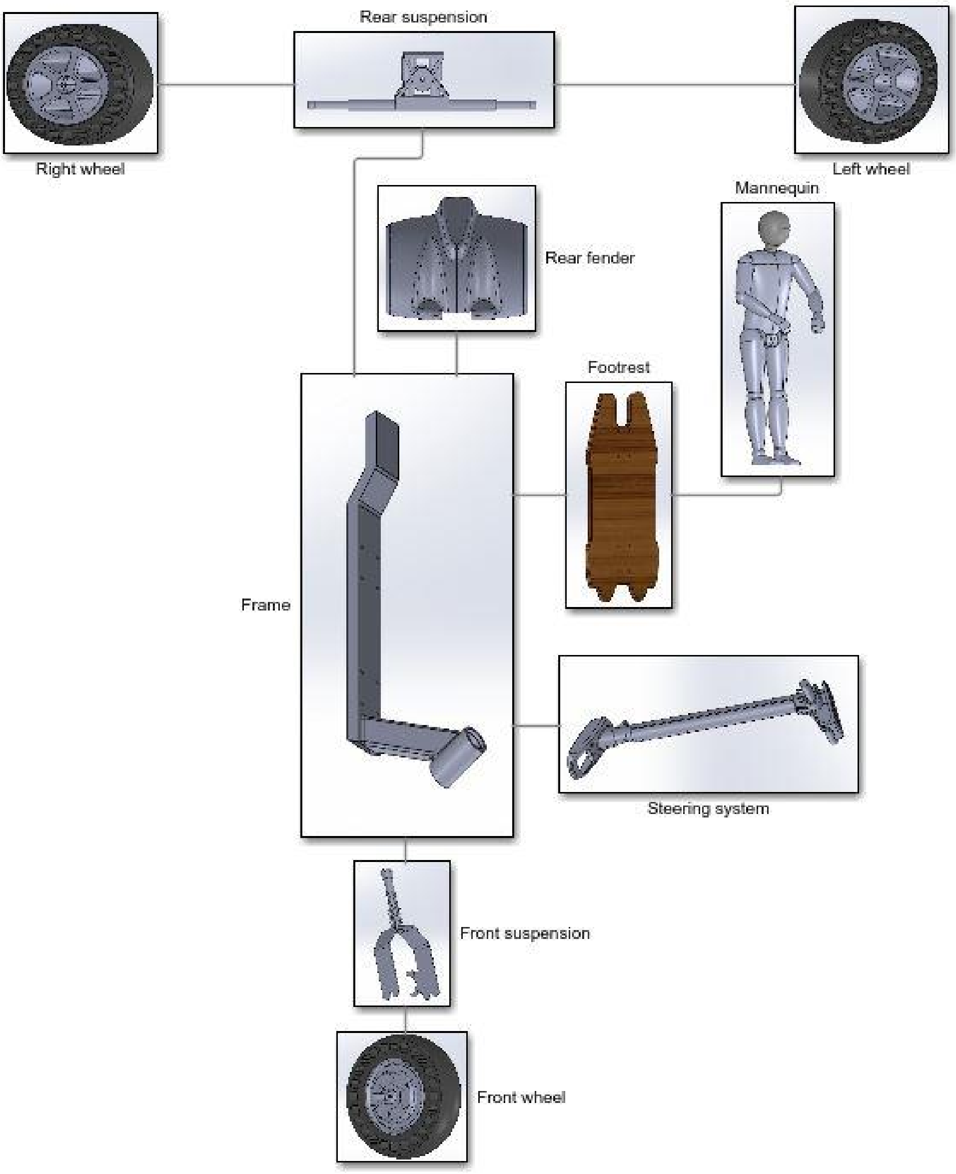

Figure 2.53 – Complete system

The complete system displayed in the three-dimensional environment Mechanics Explorer is shown in figure 2.54.

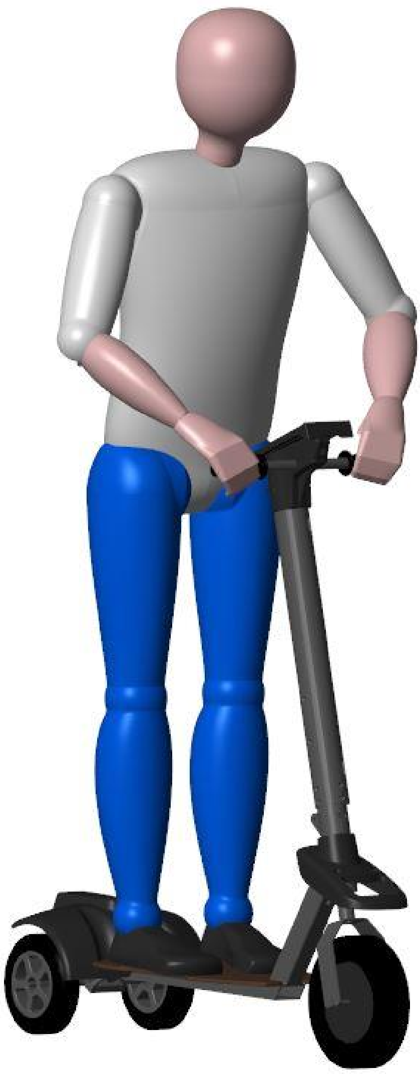

Figure 2.54 – Complete system Mechanics Explorer

Chapter 3

Experimental tests

This chapter presents the experimental tests carried out on a prototype of the vehicle. After presenting the main characteristics of the prototype used, the equipment which makes up the measurement chain for data acquisition is described. The last part shows the type of tests carried out and the post-processing of the data acquired.

3.1 Characteristics of the vehicle under test

The vehicle used in the tests was a prototype with a foam-filled front wheel and no suspension (Figure 3.1).

Figure 3.1 – Prototype front wheel

At the rear, the vehicle was equipped with two solid tyres with honeycomb geometry.

Figure 3.2 – Prototype rear wheels

3.2 Measuring chain

For vibration analysis, the measuring chain generally consists of:

- Transducer
- Pre-amplifier
- Signal conditioner
- A/D converter
- Signal analyser

The transducer is the device that converts the measurable input physical quantity to be measured into a pneumatic or electrical signal. The signal coming from the transducer, which is generally very weak, is amplified by the pre-amplifier. The latter is sent to a conditioner which performs a series of operations such as frequency filtering, further amplification, etc. The amplified and conditioned analogue signal is transformed, via an A/D converter, into a digital signal, a discrete set of numbers that can be managed by a computer.

3.2.1 Piezoelectric Accelerometer

In the case of the tests carried out on the LYNX kick-scooter, Miniature IEPE Triaxial Accelerometers manufactured by Kistler were used. In particular, the model used was type 8763B500A, shown in the figure below.

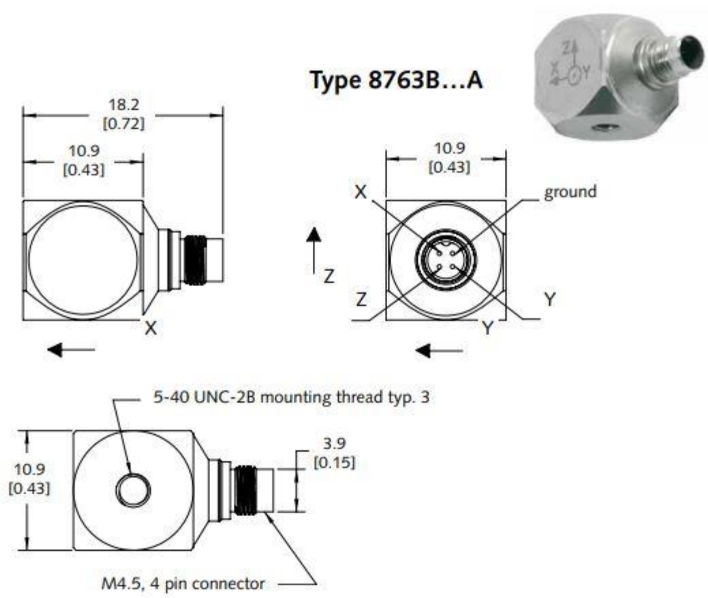

Figure 3.3 – Piezoelectric accelerometer

This is a shear accelerometer, like the one shown in figure 3.4, which can measure accelerations along three orthogonal axes in a range of ±500g, has a resonant frequency of 55 kHz and a frequency response between 1 Hz and 10000 Hz, considering a linearity error of ±5. It has a hermetically sealed, welded titanium case that allows the measurement of vibrations even underwater up to a maximum pressure of 10 bar.

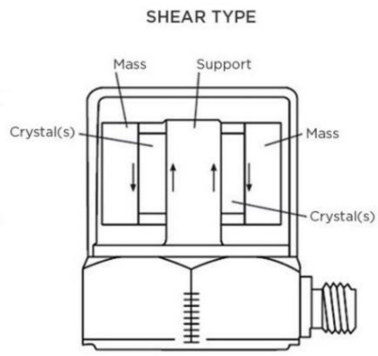

Figure 3.4 – Shear type accelerometer

This accelerometer incorporates also IEPE technology, which stands for "Integrated Electronics Piezo Electric", eliminating the need for a pre-amplifier. In this case, the measurement chain is called "Low impedance chain". The latter, shown in figure 3.5, consists of the accelerometer connected via a simple coaxial cable to an ICP power supply which is in turn connected to an acquisition system. Some acquisition systems have a built-in ICP power supply that allows further simplification of the measurement chain.

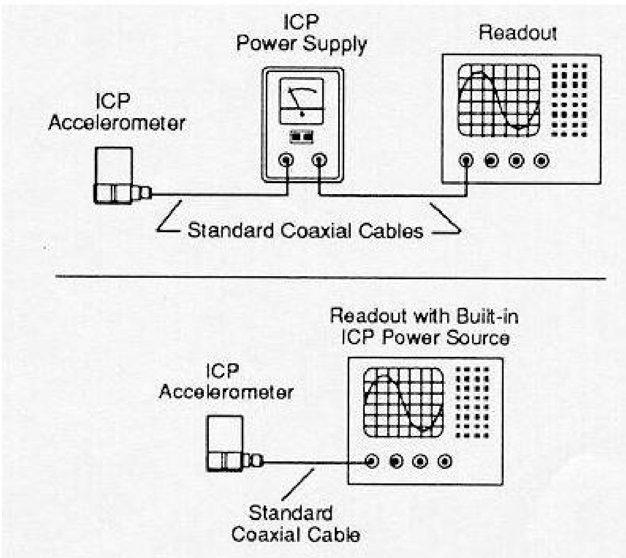

Figure 3.5 – Low impedance chain

3.2.2 Simcenter SCADAS XS acquisition system

For accelerations acquisition, a Simcenter SCADAS XS was used. This device, shown in figure 3.6, is very compact, equipped with an internal battery, and can acquire signals up to 50Khz on twelve different channels. The channels are also Voltage/ICP, which means that the device can directly power the accelerometers without the need for an external power supply.

Figure 3.6 – Simcenter SCADAS XS

The inputs, shown in figure 3.7, that this device is equipped with are:

- Twelve V/ICP Channels capable of acquiring signals up to 50khz sampling frequency. These ports are also compatible with TEDS (Transducer Electronic Data Sheets) technology. The latter allows, if the accelerometer is also compatible with this function, to automatically read transducer information that would be present on the calibration sheet such as sensitivity, model number, quantity and more. With this technology, it is therefore possible to shorten the time needed to carry out the tests, as it is not necessary to enter all the data manually and to avoid possible errors.
- One binaural headset Channel dedicated to the connection of the Siemens headset. This device is equipped with two microphones placed on both ears and has the

objective of optimising sound recording for headphone listening, in order to faithfully reproduce the sound perceptions of the listener located in the recording environment, maintaining its directional characteristics;

- One GPS Channel to track speed, with a sensitivity of $\pm$ 1 km/h, and position at a frequency of 5 Hz;
- One SPDIF (Sony Philips Digital Interface) Channel for the connection of audio devices;
- One CAN-bus Channel to read signals from different sensors in modern vehicles;
- A dual Analog Tacho Channel.

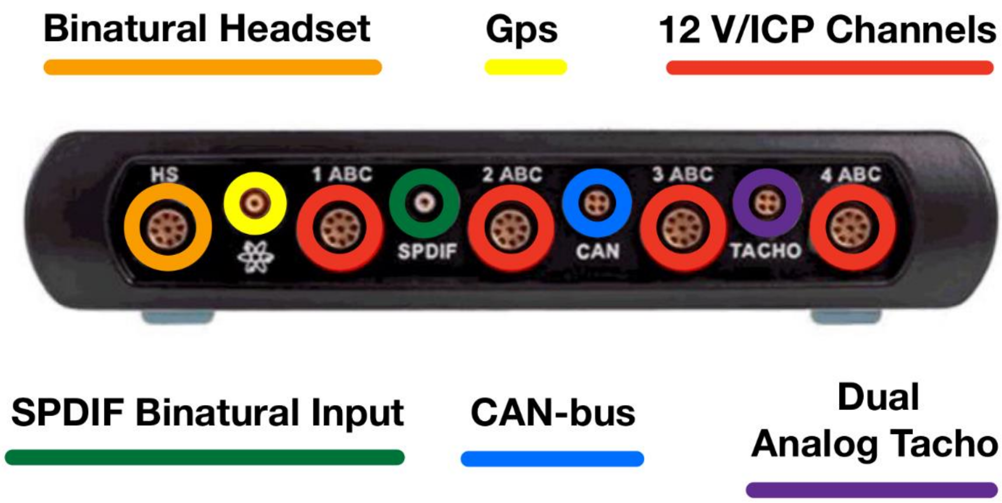

Figure 3.7 – Inputs of SCADAS XS

The connection ports located on the opposite side of the inputs, figure 3.8, through which the acquisition system can interface with other devices are:

- One micro-SD card slot;
- One LAN port through which it is possible to connect the device directly to the computer or to connect several SCADS XS using an Ethernet hub;
- One USB port to connect the device to the computer and charge the battery;

Figure 3.8 – SCADAS XS connection ports

The SCADAS XS can be used in different operation modes:

- **Frontend mode** in which the device is directly connected, via USB or LAN, to a PC equipped with Testlab LMS software;

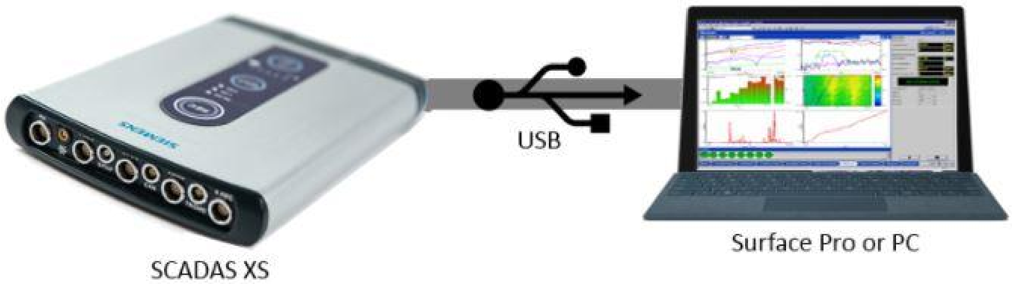

Figure 3.9 – Frontend mode

- **Tablet mode** in which the device is connected to an Android tablet equipped with the Simcenter Testlab Scope App. The connection between the tablet and the SCADAS XS is obtained through build-in Wi-Fi on the acquisition device. In this operation mode, it is necessary to insert a microSD card in the dedicated slot, on which all the data recorded by the acquisition system are saved. Through the tablet it is possible not only to visualize the data collected but also set up, start, or stop an acquisition;

Figure 3.10 – Tablet mode

- **Standalone mode** in which the device is not connected to either the PC or the tablet. In this mode, it is necessary the presence of the microSD card with a preloaded measurement template. The measurement setup is configured using Siemens Testlab software and the generated file is exported to the microSD-card. In this mode of use, tests can be started and stopped using the build-in REC button. The latter has an LED through which the status of the device can be monitored. The collected data are saved on the microSD card and can be exported to a large number of third-party formats.

3.3 Experimental setup

To measure vibrations, three IEPE accelerometers, described in the previous paragraph, were placed:

- One at the centre of the footrest;

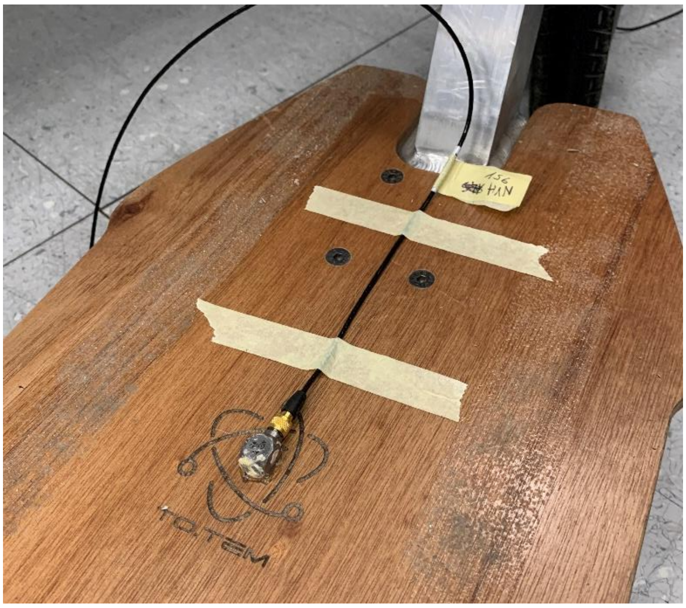

Figure 3.11 – Footrest accelerometer

- One on the fork;

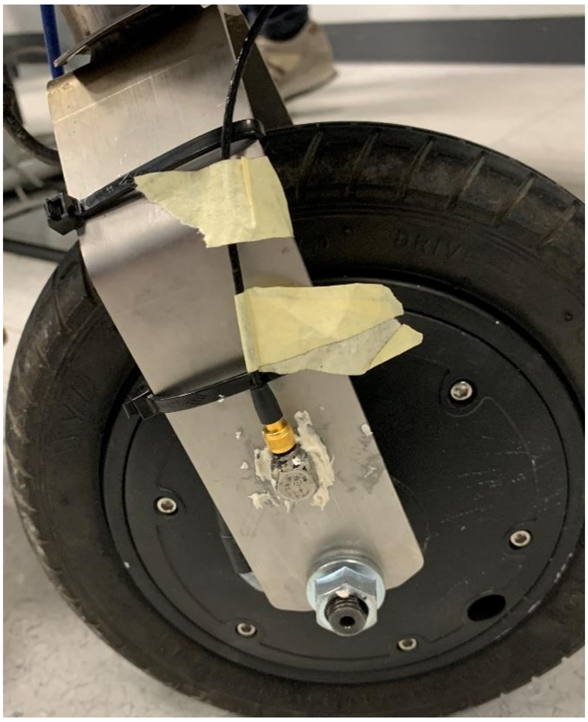

Figure 3.12 – Fork Accelerometer

- One on the steering dashboard.

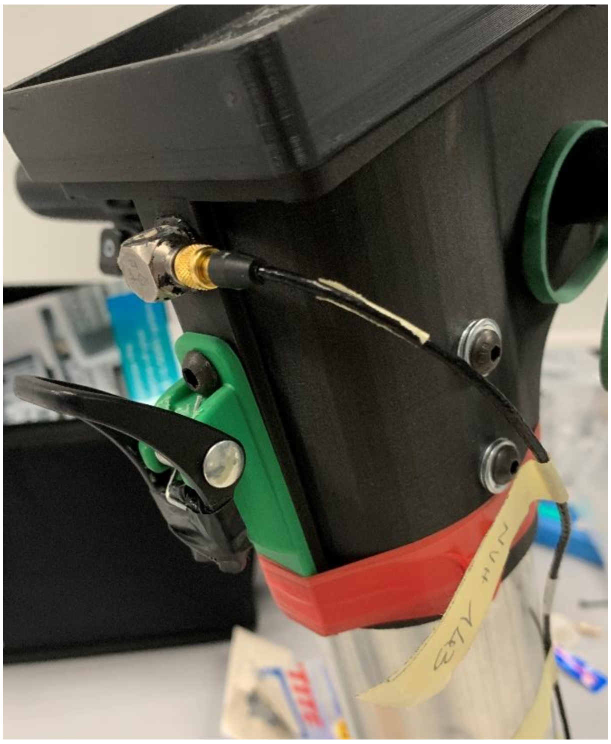

Figure 3.13 – Dashboard accelerometer

Mounting of accelerometers is essential for reliable and accurate measurements. A thin layer of beeswax was used for the transducers mounted on the footplate and dashboard, while an adhesive suitable for coupling with steel was used for the fork transducer. This mounting method slightly reduces the resonance frequency, but it is not a problem in this case due to the high bandwidth of piezoelectric accelerometers and the low frequency of the phenomena to be measured.
Since the SCADAS XS has V/ICP ports that directly power the IEPE transducers, no power supply is required for the connection between the accelerometers and the acquisition system, but only two cables:

- The first is a 4-pin to 3 BNC cable, shown in figure 3.14. The 4-pin connector plugs in directly to the accelerometer;

Figure 3.14 – 4 PIN to 3 BNC cable

- The second is a three BNC to one LEMO cable, shown in figure 3.15. With this cable, it is possible to connect the three channels of a triaxial accelerometer to a single V/ICP port on the SCADAS XS.

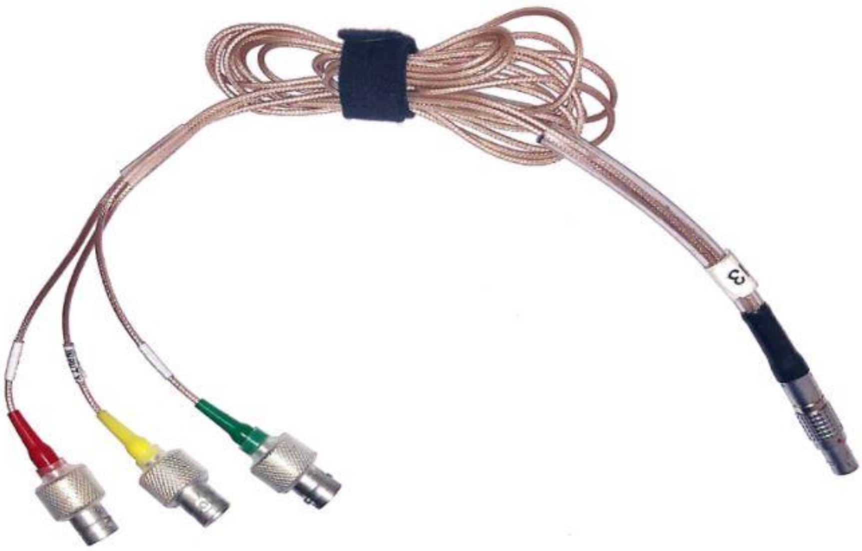

Figure 3.15 – LEMO cable

The two cables are then linked together using the BNC connectors by matching the corresponding axis on each cable marked on the wires with a label.

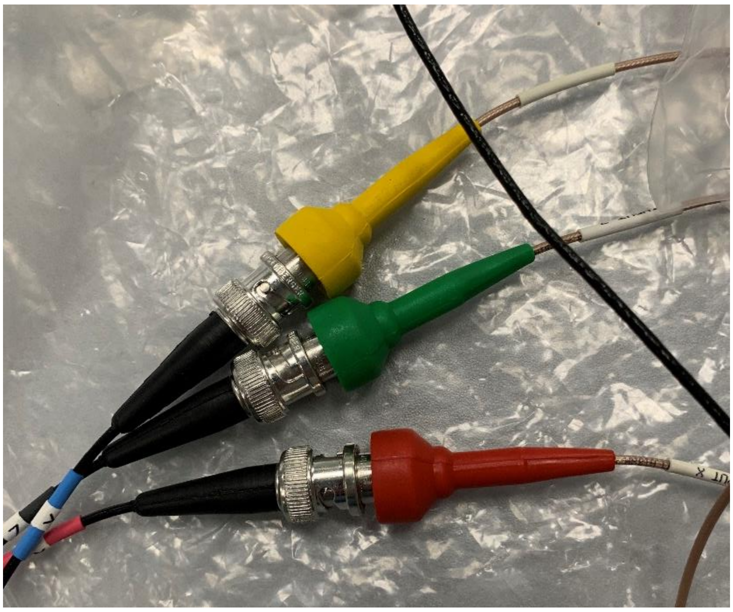

Figure 3.16 – BNC connection

Finally, the cable is connected to the SCADAS XS via the LEMO connector.

Figure 3.17 – SCADAS XS connection

The acquisition system was then fixed on the dashboard with rubber bands and tape.

Figure 3.18 – SCADAS XS mounting

The final experimental setup is shown in figure 3.19.

Figure 3.19 – Instrumented vehicle

The final measurement chain used for acceleration acquisitions on LYNX is shown in figure 3.20.

Figure 3.20 – Final measurement chain

The measurement chain consists of the IEPE accelerometer which measures the accelerations and the acquisition system that collects the data via the micro-SD card and directly powers the transducer without the need for an amplifier. The recorded data can be analysed and post-processed through the use of a laptop with dedicated software such as Simcenter Testlab.

3.4 Simcenter Testlab

For the tests on LYNX, it was decided to use the SCADAS XS in standalone mode, without connecting the device to the computer, but saving the data directly on the micro-SD card. To perform measurements in this mode, a template must be present on the micro-SD card. A template is a file where are stored all the custom test settings. To create one, Simcenter Testlab was used.

After creating a new project, it is possible to create custom tests into the "Channel Setup" worksheet, shown in figure 3.21. This table resembles an excel sheet in which each row represents one of the physical channels of the acquisition system. From figure 3.21 it can be seen that nine channels were enabled representing the three orthogonal directions of the three accelerometers mounted on the vehicle.

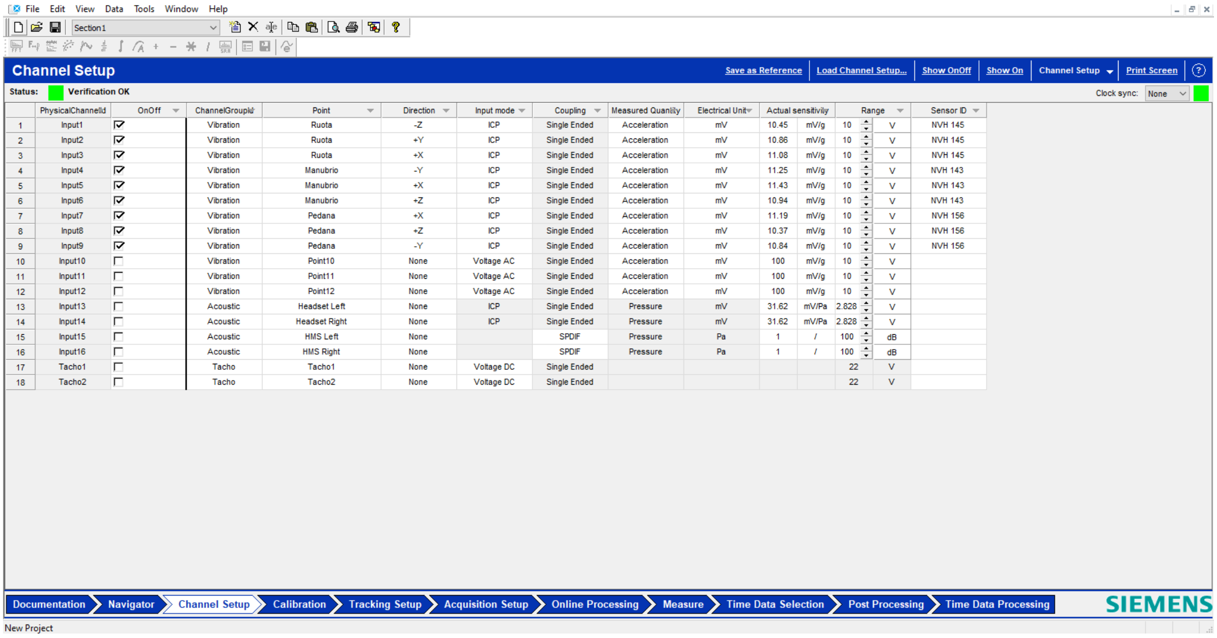

Figure 3.21 – Siemcenter Testlab Channel Setup

There are eleven columns in which to enter the parameters:

- **On-Off** with which it is possible to enable or disable the input;

- **Channel Group Id** is an identification term to indicate which group the channel belongs to. Available options are: vibration, acoustic, tacho and others. In the case under study since only accelerometers were connected, the vibration option was selected in all the lines;

- **Point** is a free description field where anything can be entered. In the case of input 1, the word "Ruota" was chosen as the accelerometer was positioned on the fork;

- **Direction** whose selections are +X, -X, +Y, -Y, +Z, -Z. Each accelerometer has its own reference system whose directions are shown on the transducer case, as shown in figure 3.22;

Figure 3.22 – Accelerometer reference system

For the execution of the tests, a predefined coordinate system was defined, illustrated in the figure below.

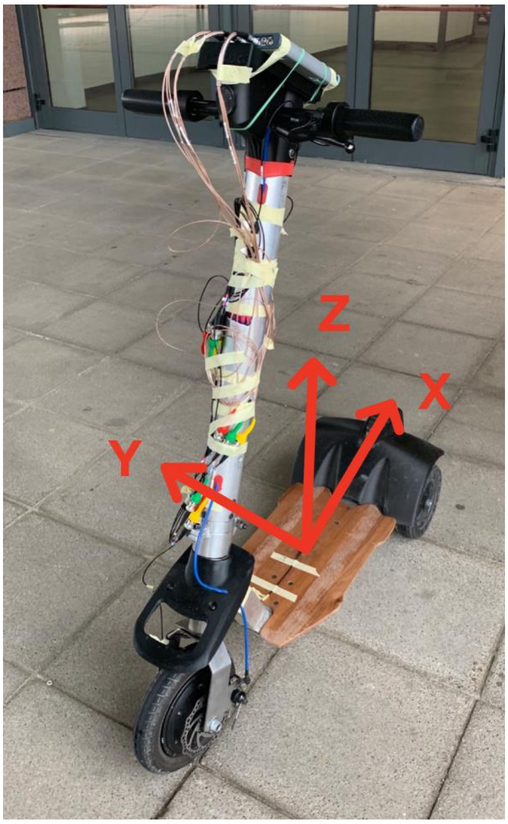

Figure 3.23 – Global coordinate system

From figure 3.23, it can be seen that the x-axis is facing longitudinally towards the rear of the vehicle, the z-axis in a vertical direction facing upwards and the y-axis in a lateral direction. Figure 3.24 shows the two reference systems in the case of the footplate, the global one marked on the tape and that of the accelerometer in red. Taking as reference the inputs 7, 8 and 9 that refer to the accelerometer positioned on the footrest (Fig. 3.25), we can see that:

- in line 7, which corresponds to the x-axis of the transducer, the option +X was selected, since the two axes have the same direction and the same orientation;
- in line 8, which corresponds to the y-axis of the transducer, the +Z option was selected because the two axes have the same direction and the same orientation;
- in line 9, which corresponds to the z-axis of the transducer, the -Y option was as the two axes have the same direction but opposite orientation;

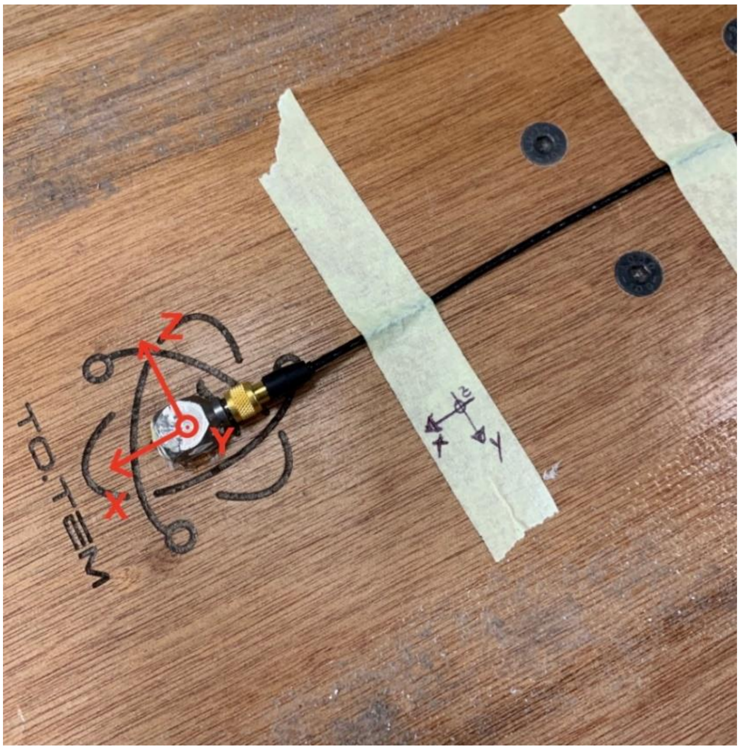

Figure 3.24 – Footrest accelerometer

7	Input7	☑	Vibration	Pedana	+X	ICP	Single Ended	Acceleration	mV	11.19	mV/g	10		V	NVH 156
8	Input8	☑	Vibration	Pedana	+Z	ICP	Single Ended	Acceleration	mV	10.37	mV/g	10		V	NVH 156
9	Input9	☑	Vibration	Pedana	-Y	ICP	Single Ended	Acceleration	mV	10.84	mV/g	10		V	NVH 156

Figure 3.25 – Footrest setup

The same procedure was used for the other accelerometers in order to obtain the global reference system shown in figure 3.23;

- **Input mode** in which the available options are Voltage AC, Voltage DC and ICP. In the case under consideration, the field was set to ICP because all accelerometers used were IEPE. In this way the SCADAS XS directly powers the transducer without the need for an external amplifier;

- **Coupling** indicating the connection mode, for each accelerometer the single ended option was selected;

- **Measured quantity** indicates the type of physical quantity to be acquired. In this case, the acceleration option was selected for all channels;

- **Electrical unit** indicates the unit of measurement output from the channel. Since all the accelerometers used were IEPE, the output quantity is a potential difference in mV;

- **Actual sensitivity** indicates the output voltage generated by a 1 g force. This value is different for each axis and can be found on the calibration sheet of the transducer. In the case of the accelerometers used, a feature called TEDS (Transducer Electronic Data Sheet) is available whereby the acquisition system can automatically read some of the transducer's parameters, such as sensitivity, and enter them directly into the appropriate fields. To use this function in Testlab, in the "Channel Setup" section there is an option called "Read Teds" as shown in the figure below;

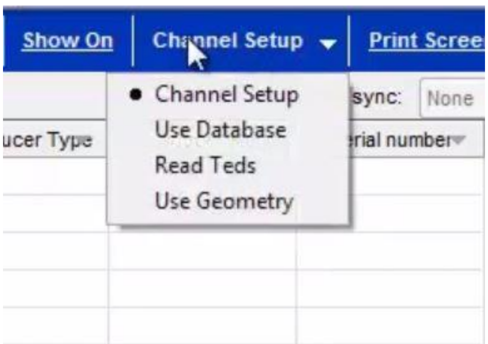

Figure 3.26 – Teds option

- **Range** indicates the voltage interval. In the case under consideration, since type b500 accelerometers were used, the calibration sheet reports a voltage output of ±5V, and therefore a range of 10V;

- **Sensor ID** is a transducer identification term.

After filling in all the fields in the channel options tab, in the acquisition setup tab other parameters have been defined, the most important of which are the acquisition frequency set to 25600 Hz and the measurement time set to 30 s, a much longer time than necessary so that measurements can be started and stopped directly using the dedicated button on the SCADAS XS. The template was then saved on the micro-SD card which was inserted into the acquisition system.

3.5 Wheel stiffness estimation

This section describes how the stiffness of the rear wheels was estimated. The idea behind this test is to apply a known vertical load in the centre of the wheel and from the measurement of the deformation obtain the stiffness.

Figure 3.27 – Vertical stiffness test setup

As can be seen from figure 3.27, there is a structure that is fixed on one side and bolted to the wheel centre on the other side. After checking that the structure was flat with a spirit level, weights of 10 kg were applied in sequence up to 40 kg and, for each step, the distance of the wheel centre from the ground was measured using a gauge, from which the deformation of the wheel was calculated. The values obtained from the test were reported in Matlab, and a linear interpolation was performed using the “fit” function, from which an estimated value of vertical stiffness was obtained.

The graph below shows the experimental results with blue dots and the fit curve in red. It can be seen that the experimental data can be approximated very well as a straight line whose slope represents the vertical stiffness of the wheel. The estimated static stiffness value is 87 N/mm.

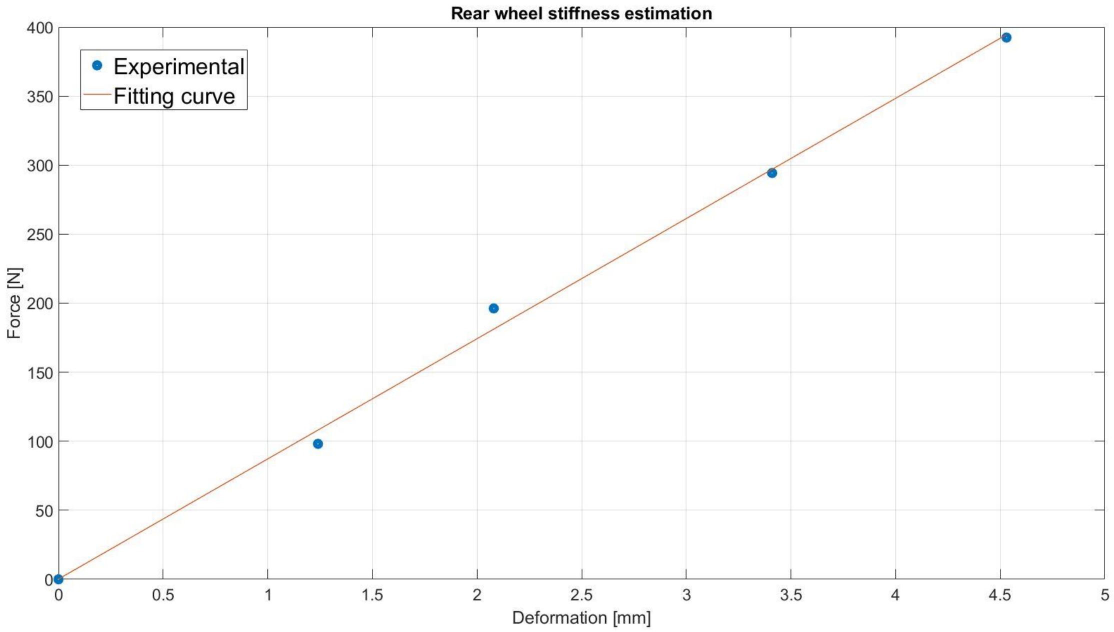

Figure 3.28 – Rear wheel stiffness estimation

It was not possible to perform the same operation on the front wheel as the only one available was already mounted on the vehicle. In this case, the stiffness value was estimated by performing a calibration with the experimental data.

3.6 Road test

The experimental test carried out on the vehicle was passing over speed bumps placed on a cycle path as shown in the figure below.

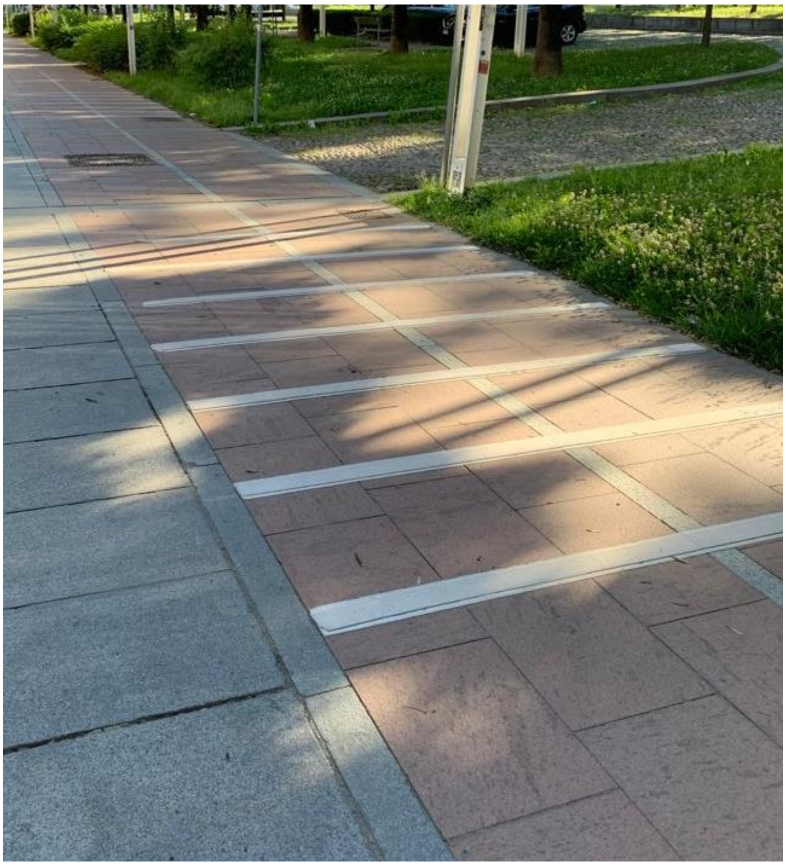

Figure 3.29 – Speedbumps

As can be seen from figure 3.29, there are two sets of speed bumps consisting of seven steps, each two millimetres high and eight centimetres long, spaced sixty-five cm apart. The test was performed at two different speeds 6 km/h and 11 km/h, and two repetitions were carried out for each. To start each test, the first operation was to press the REC button on the SCADAS XS, whose led changes from blue to red when it starts to acquire. The vehicle was then driven along a stretch of road to reach the desired speed, after which the two sets of speed bumps were traversed at a constant speed. At the end of the test, the REC button was pressed again, stopping the acquisition of accelerations, and saving the data file directly on the micro-SD card.

3.7 Post processing and export of data

After testing, the acceleration data measured by the accelerometers were transferred from the micro-SD card directly to the PC for post-processing. A low-pass filter was applied to the raw data at 250 Hz and 50 Hz using Simcenter Testlab. Within the programme, it is possible to use the time signal calculator, in which the conditioning tab contains several filters.

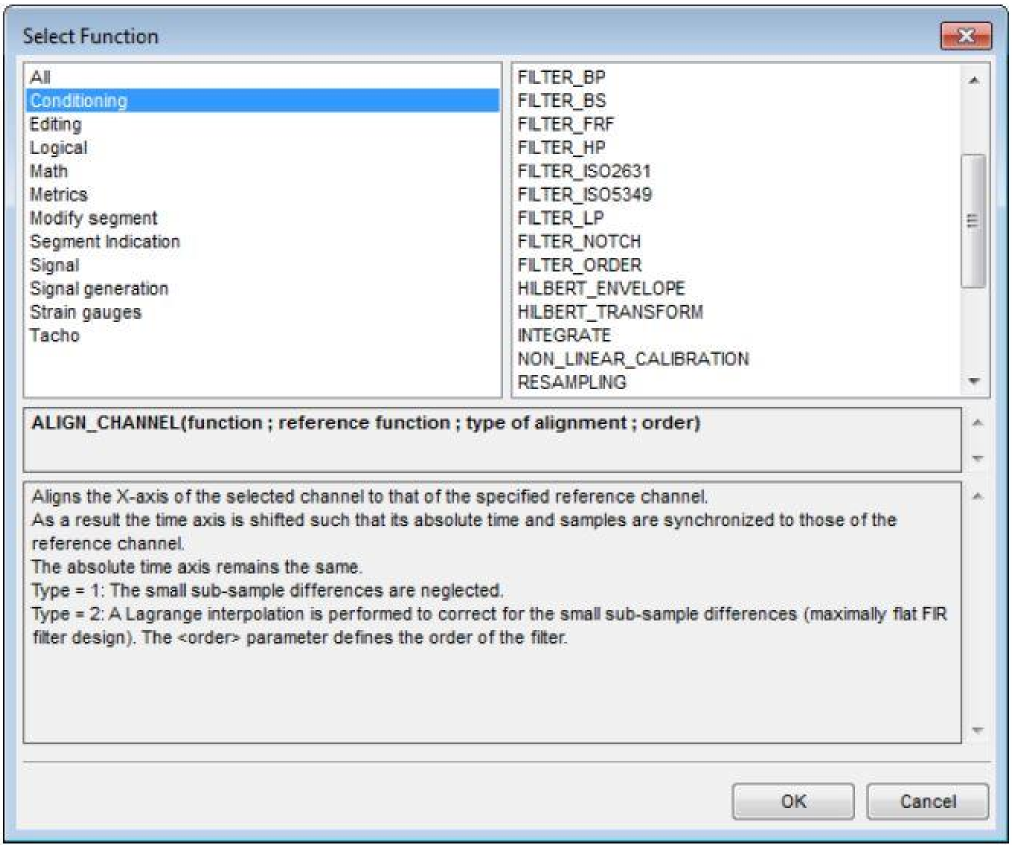

Figure 3.30 – Time signal calculator functions

After selecting the LP filter, a window opens in which it is possible to change some parameters including cut-off frequency, filter type and order. The “Show” button can be used to visualize the filter shape, phase, and group delay.

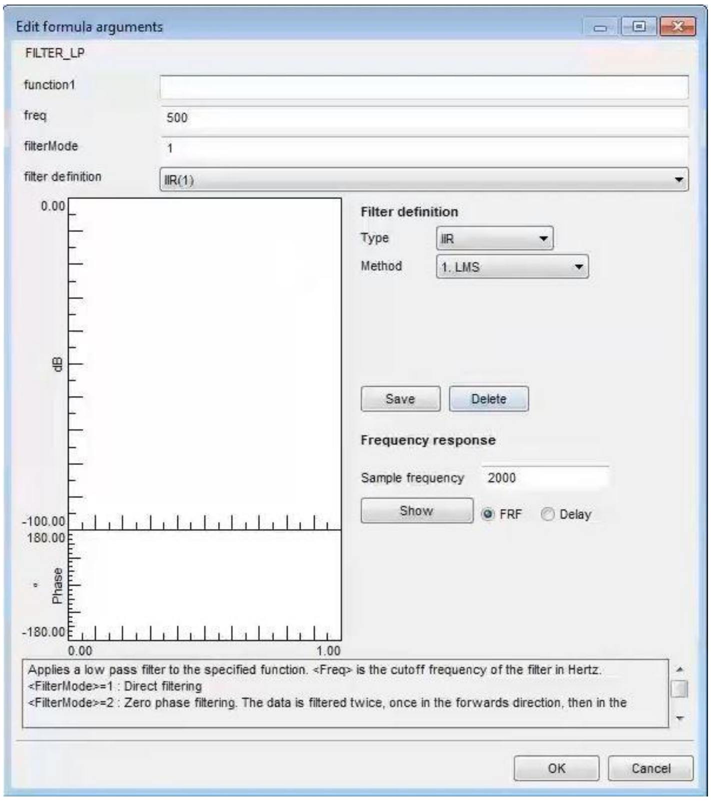

Figure 3.31 – Low pass filter interface

In this case, a Finite Impulse Response (FIR) filter was used, first at 250 Hz and then at 50 Hz. In the following figures, it is possible to see the accelerations in the test at 11 km/h acquired by the accelerometer placed on the handlebar along the z-axis, unfiltered, after applying the filter at 250 Hz and after applying the filter at 50 Hz.

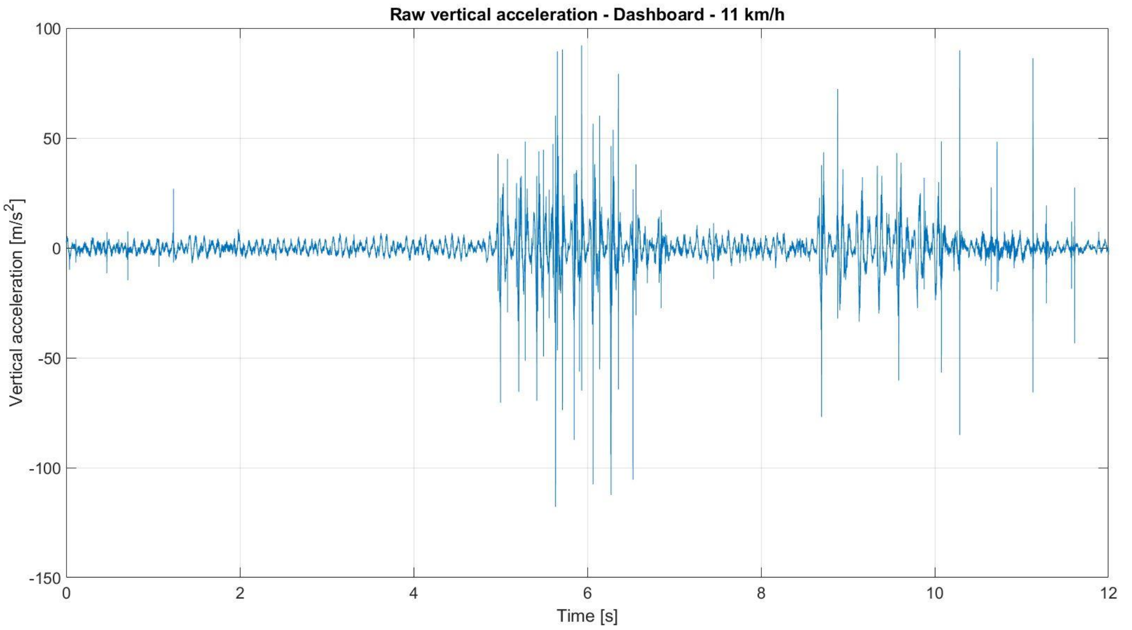

Figure 3.32 – Raw vertical acceleration dashboard

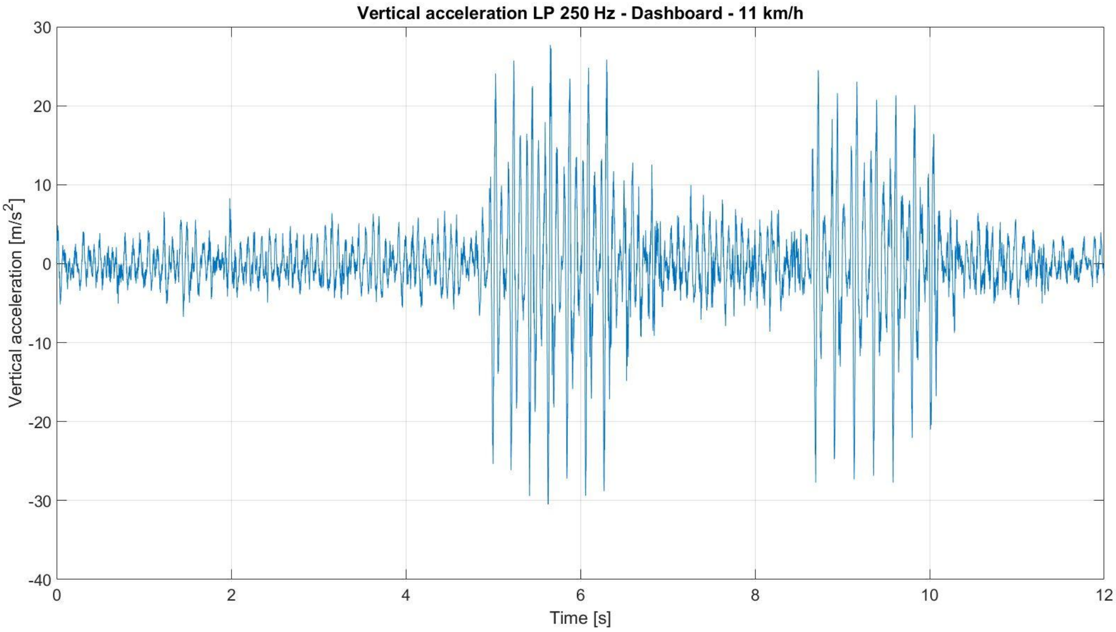

Figure 3.33 – Vertical acceleration LP 250 Hz dashboard

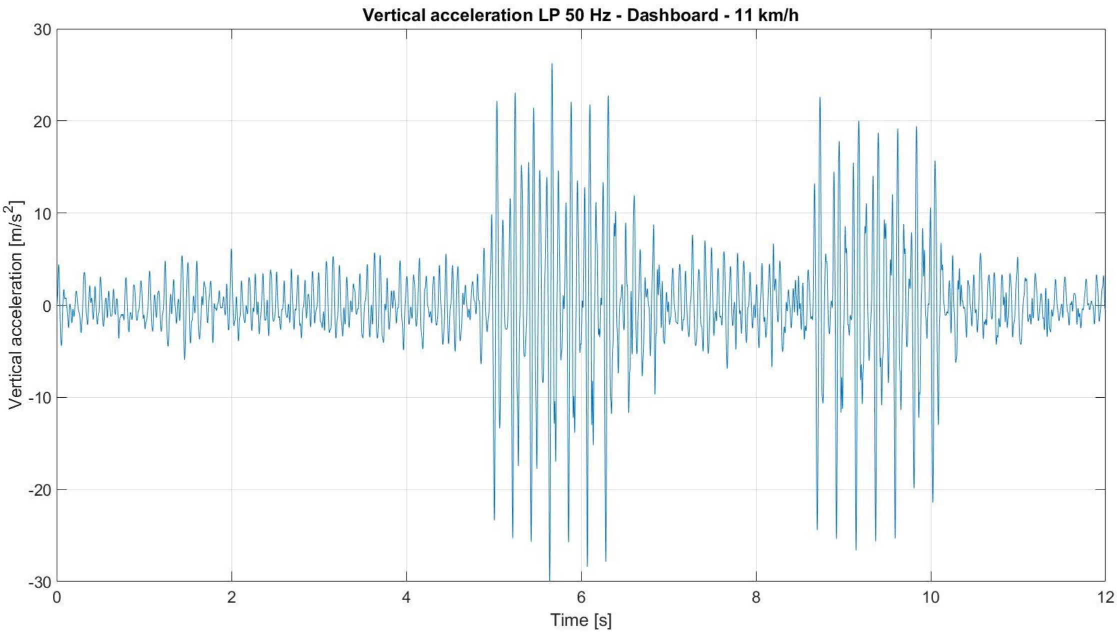

Figure 3.34 – Vertical acceleration LP 50 Hz dashboard

As can be seen in graph 3.32, since the acquisition frequency was set very high, there are very high peaks in the raw data when passing over the speed bumps, which could be due to numerous factors such as the driver's hands hitting the handlebars. Looking at the results filtered at 250 Hz and 50 Hz, it is noticeable that the signal is much cleaner and smoother.

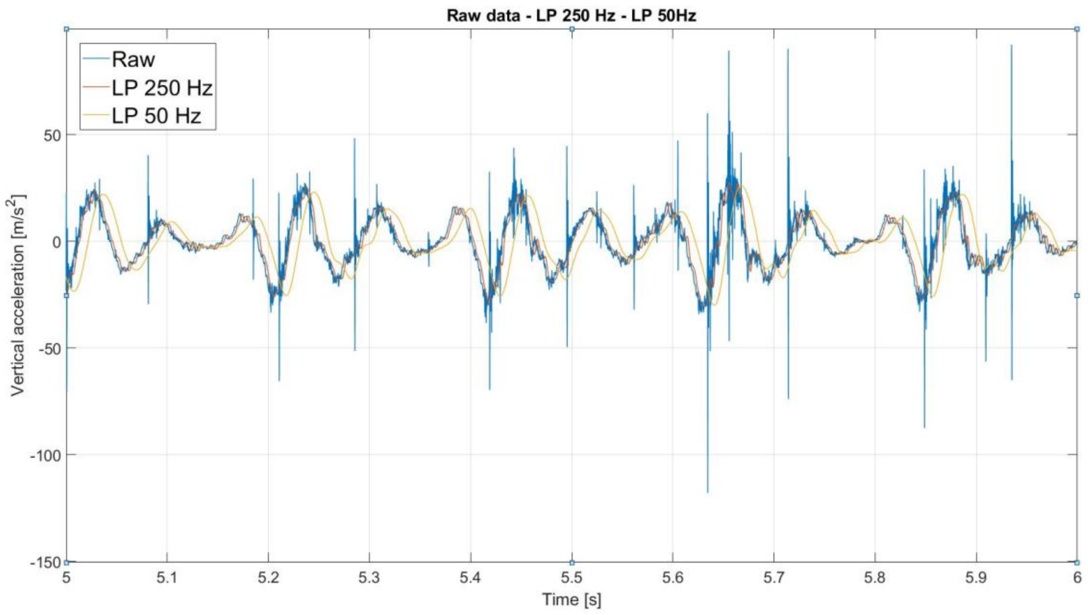

Figure 3.35 – Comparison of vertical acceleration

In the graph above, the three signals are superimposed, and it can be seen that the introduction of the low-pass filter introduces a delay due to the fact that before the filter produces an output, a number of data samples from the input signal must pass through.
Since a FIR filter was used, the delay is constant at all frequencies and can be cancelled.
In the case under consideration for the low-pass filter at 250 Hz, the delay is 0.003 s while for the low-pass filter at 50 Hz, the delay is 0.013 s.
After post-processing of the data, the results can be exported to Matlab using the dedicated function in Simcenter Testlab. This function creates a signal variable in Matlab as shown in figure 3.36.

Figure 3.36 – Test Matlab signal

In the signal are present:

- The values along the x-axis which in this case are the time values;
- The values along the y-axis which in this case are the measured acceleration values. In particular, there are twenty-seven columns, each of which represents a channel, considering the nine channels repeated for raw data, filtered at 250 Hz, and filtered at 50 Hz.
- The function record containing additional information such as the name of the different channels, the date of creation, etc.

Chapter 4

Comparison between experimental data and model results

In this chapter, the data collected in the experimental tests described in the previous chapter are compared with those calculated by the model. The number of tests carried out is limited and the lack of wheel data makes the calibration of the model very complicated. Furthermore, there are a series of parameters that cannot be taken into account, such as the variation of the position of the centre of gravity due to the movement of the driver during the ride, or even the forces exchanged between the vehicle and the driver on the steering and the footrest. The purpose of this chapter is to demonstrate that the dynamic behaviour of the model correctly simulates what happens in reality and to see qualitatively the impact that the introduction of the front suspension or the change of some parameters has on the vehicle.

4.1 Experimental test results

In this section, the experimental test results for both tests at two different speeds are presented and commented on. All graphs shown refer to accelerations filtered with the 50 Hz low-pass filter.

4.1.1 Experimental data - 6 km/h

Figure 4.1 shows the superimposed accelerations along the z-axis acquired by the accelerometers placed on the steering and the fork.

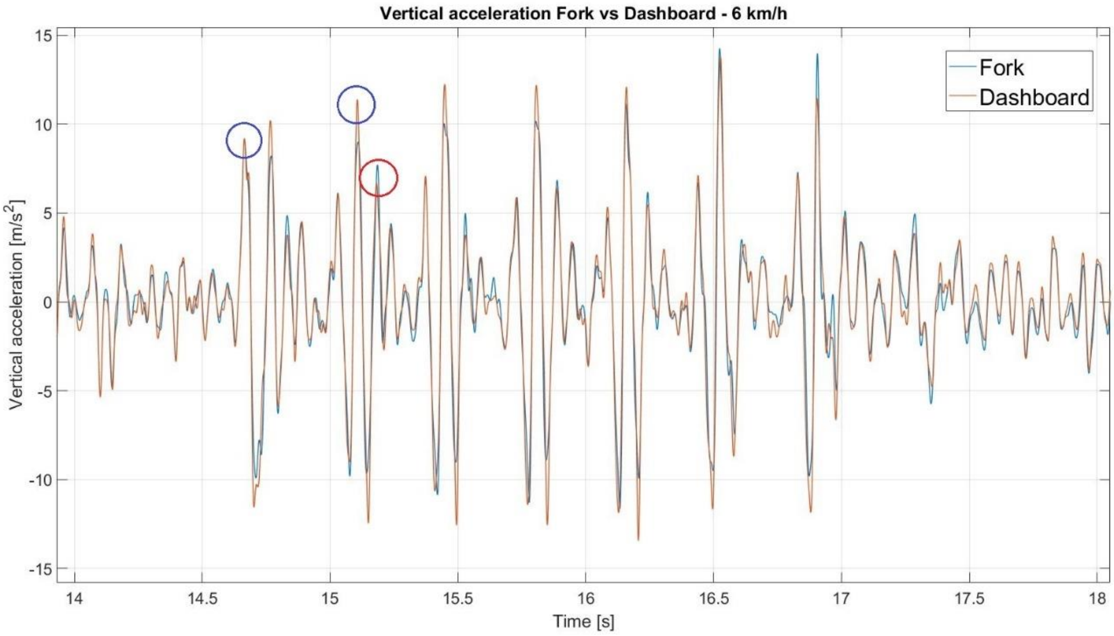

Figure 4.1 – Experimental vertical acceleration fork vs dashboard at 6 km/h

From this graph it can be seen that the first two peaks, highlighted with blue circles, are due to the impact of the front wheel with the speed bumps, in fact, the wheelbase of the vehicle is eighty centimetres while the distance between two steps is sixty-five centimetres. This is followed by the impact of the rear wheels, highlighted with a red circle, and continues with the alternation between the front and rear, ending with two collisions on the rear wheels. Comparison of the accelerations measured on the steering and those measured on the fork shows that the trends and values are practically the same, indicating that the vibrations are transmitted rigidly, as assumed in the model.
The situation for accelerations measured on the footplate is different. From graph 4.2, in which the accelerations measured on the steering wheel are compared with those on the footrest, it can be noted that the accelerometer placed on the platform is more sensitive to rear wheel impacts, in fact, the highest peaks occur from the second impact of the front wheel, highlighted with a blue circle, when the rear wheel starts to hit the speed bumps.
In the last impacts, it can be seen that this tendency tends to decrease, but this also depends on the variability in the transition from one step to the other.

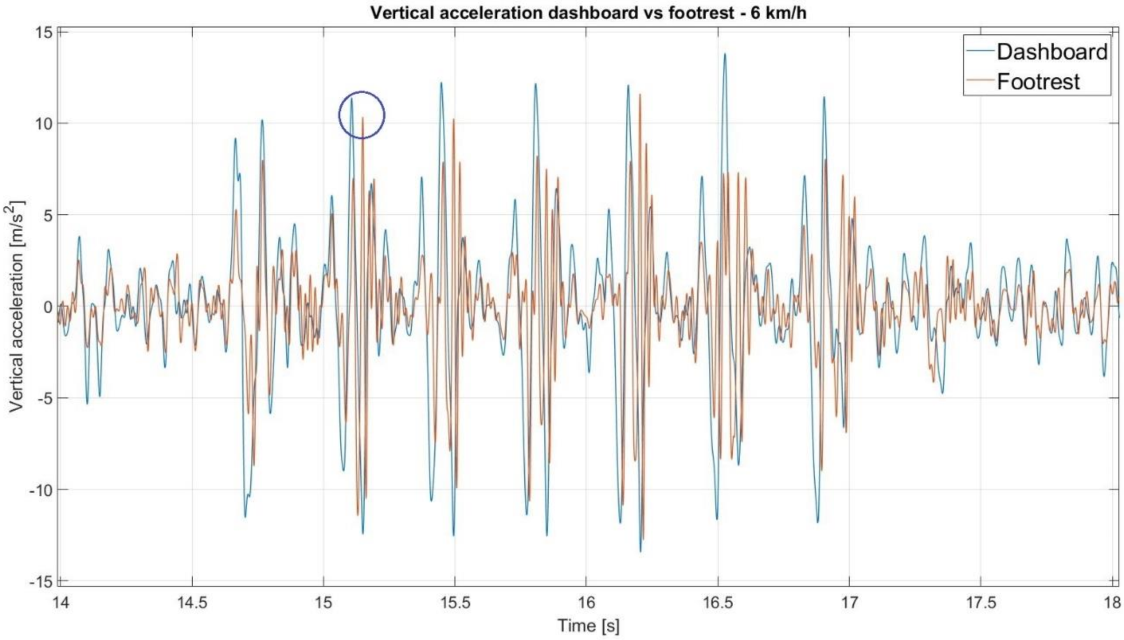

Figure 4.2 – Experimental vertical acceleration dashboard vs footrest at 6 km/h

4.1.2 Experimental data - 11 km/h

As in the previous paragraph, figure 4.3 shows that the accelerations measured on the fork and those measured on the steering are almost identical even when the speed is doubled.

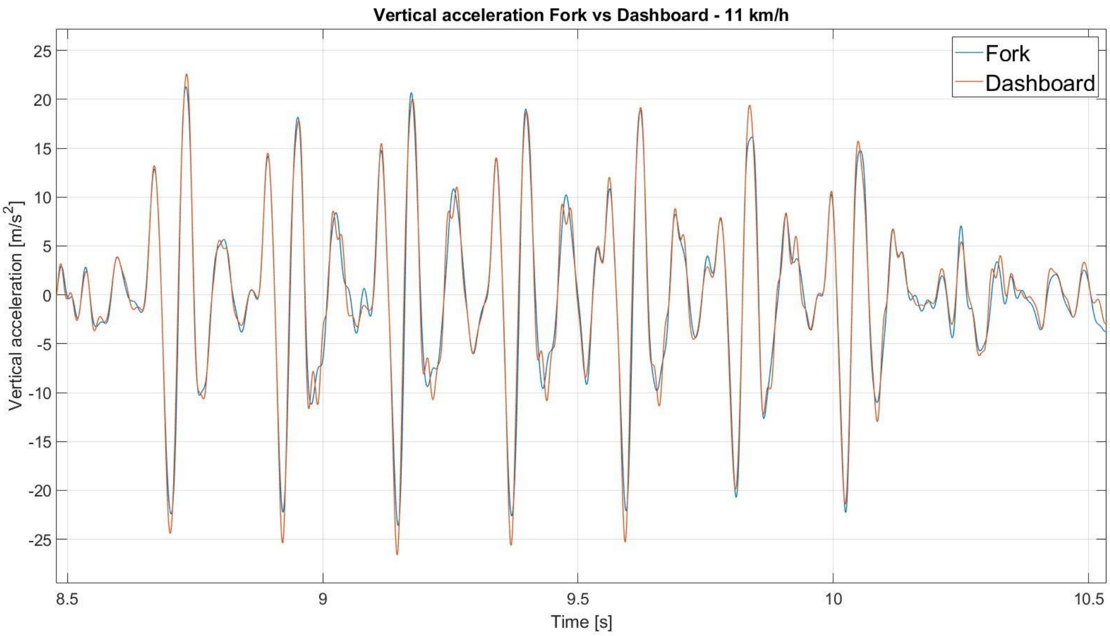

Figure 4.3 – Experimental vertical accelerations fork vs dashboard at 11 km/h

Comparing the graph above with the one at 6 km/h, it is possible to assert that doubling the speed also approximately doubles the vertical acceleration.
Even for the 11 km/h test, the same conclusion as in the previous paragraph can be reached that the accelerometer on the footrest is more sensitive to rear wheel impacts.

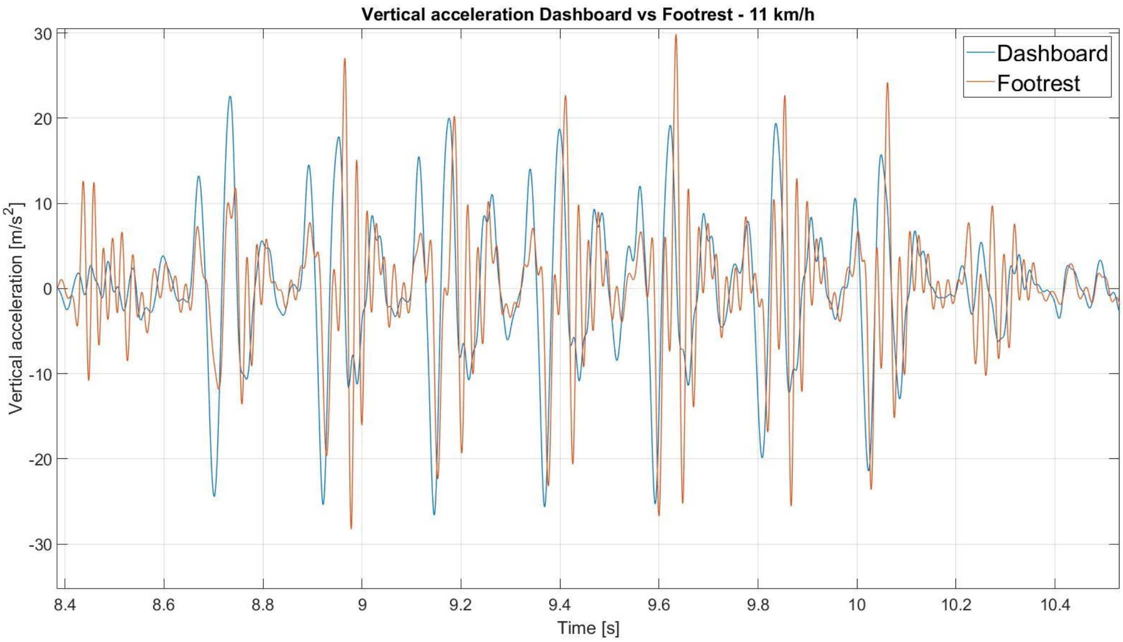

Figure 4.4 – Experimental vertical acceleration dashboard vs footrest at 11 km/h

4.2 Model configuration

In this section, the vertical accelerations measured by the accelerometers are compared with those calculated by the model by carrying out the same tests as in reality.

Before performing the simulations, some parameters were set. A variable step solver (ode15s) was used with a maximum step of 0,001 s and a relative tolerance of 0,01%.

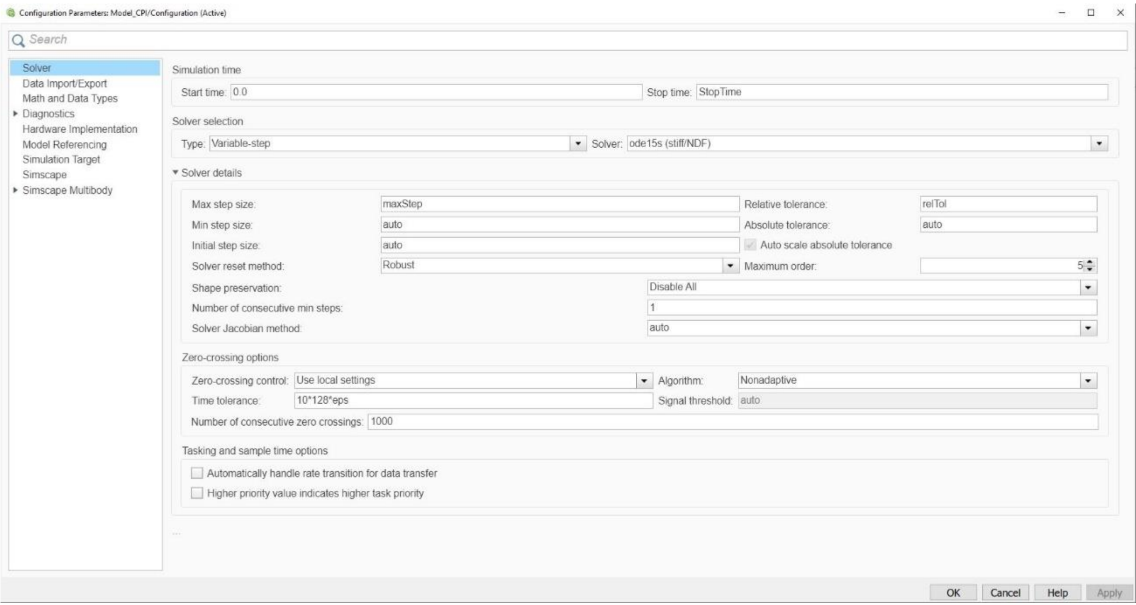

Figure 4.5 – Model settings

Although a variable step solver was utilised, a constant acquisition frequency was set equal to that used in the experimental tests of 25600 Hz. To set this option, in the "Data Import/Export" tab, in the "Additional parameters" section, an Output times vector with a period $T = \frac{1}{F_s}$ was inserted.

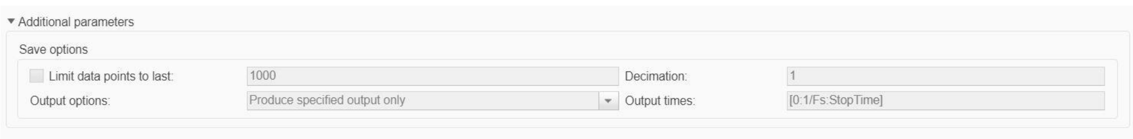

Figure 4.6 – Model acquisition frequency

For all the simulations carried out, the CPI model, described in section 2.4.3, was used. In order to replicate the experimental tests, it is necessary to model the same obstacles that are present in reality. As explained in paragraph 2.4.3, to provide a road input it is necessary to insert the elevations along the z-axis of the road profile as a function of the x dimension into the look-up table within the subsystem used for the calculation of the vertical force of the wheel.

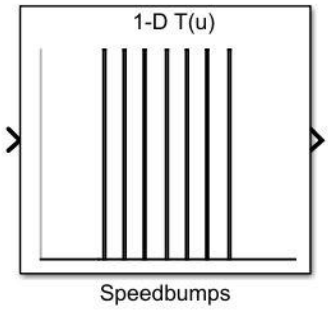

Figure 4.7 – Road profile

As can be seen from figure 4.7, there is a flat section necessary for the vehicle to reach the desired speed, then there are the seven steps in a row with a height of two mm.
The other parameters set before launching the simulations were the stiffness and damping of the wheels:

- For the rear wheels, the stiffness value used was the one estimated in the experimental test described in paragraph 3.5, equal to 87 $\frac{N}{mm}$. The damping value was estimated by iteration and set to 800 $\frac{N}{m/s}$;
- For the front wheel, no data was available, and the values were obtained through iteration by calibrating the model on the experimental data. The estimated values are 139 $\frac{N}{mm}$ for the stiffness and 750 $\frac{N}{m/s}$ for the damping.

For all comparisons made between model and experimental data, the accelerations measured on the steering dashboard were used.

4.2.1 Test comparison - 6 km/h

In figure 4.8, the accelerations measured by the accelerometer on the dashboard are compared with those calculated on the model in the time domain.

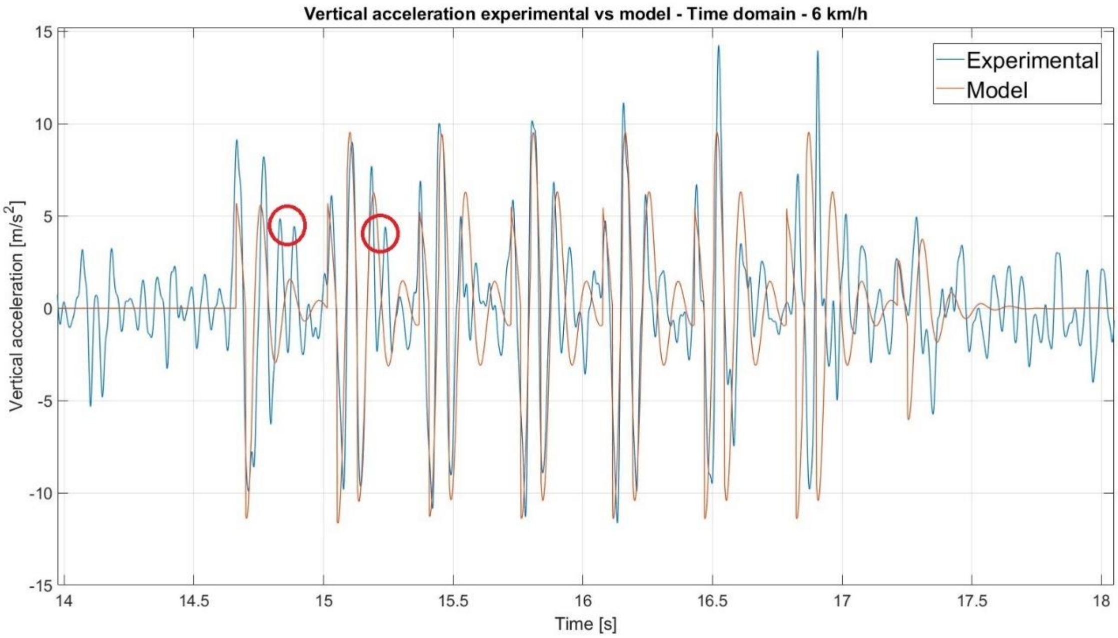

Figure 4.8 – Vertical acceleration experimental vs model in time domain at 6 km/h

As can be seen from the graph above, the trend and absolute values of the accelerations in the time domain are very similar. Red circles highlight points where the experimental oscillation frequency is higher than that of the model. This phenomenon is due to the fact that, in some cases, between one step and another there are the joints of the tiles that make up the path of the cycle track, which constitute a source of oscillation that is not present in the model. This effect can also be noted before passing the speed bumps where there is a fairly clear vibration pattern due to these inputs. From the graph, it can be also seen that the latest impacts are slightly out of phase in time when comparing model and experimental tests. This variation is caused by the fact that in reality, in the tests, the speed value was not perfectly constant, as in the model. To improve the accuracy of the simulation even more, a tachometer could be added to the acquisition system in order to have the speed value during the whole test.

The similarity of the two signals can also be seen in the frequency domain, whose graph is shown in figure 4.9, where it can be noted that the frequencies and the amplitude of the oscillations are very similar between experimental and model.

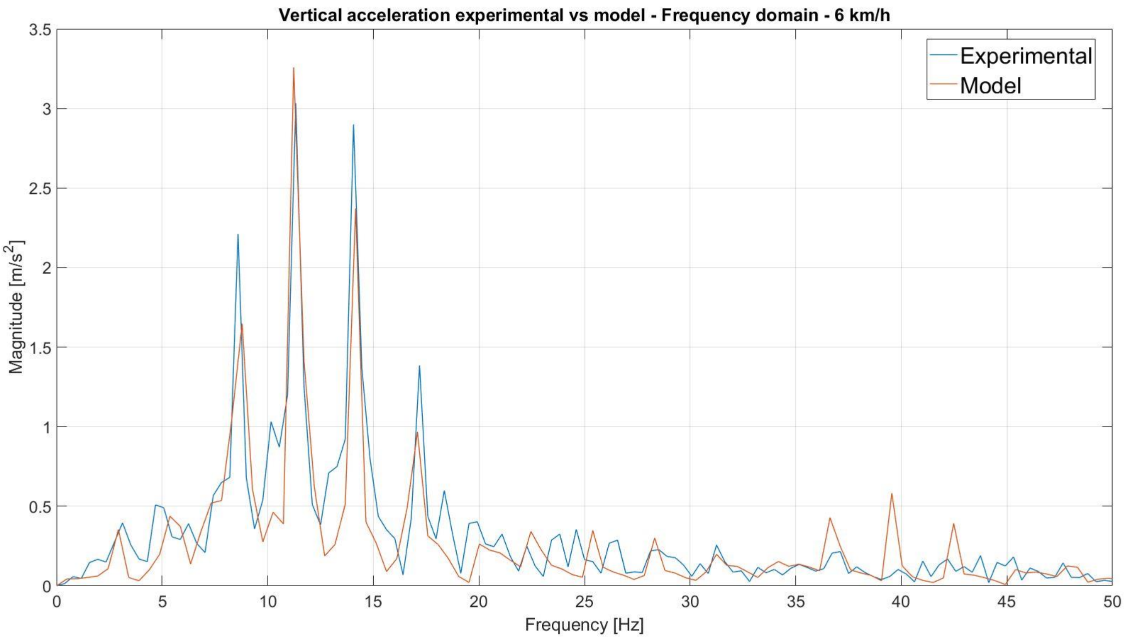

Figure 4.9 –Vertical acceleration experimental vs model in frequency domain at 6 km/h

When comparing the vibrations in the time and frequency domains, it is possible to note that the model is not perfect, but it simulates quite correctly what happens in reality. Looking at the 4.8 graph, it is evident that while in the model the behaviour remains constant from one step to the next, in reality, there are fluctuations in the measurements, as can be seen in the last two frontal impacts, where the measured value is higher than in the previous ones.

4.2.2 Test comparison - 11 km/h

As in the previous paragraph, the first figure represents the comparison between the experimental accelerations and those of the model on the handlebar.

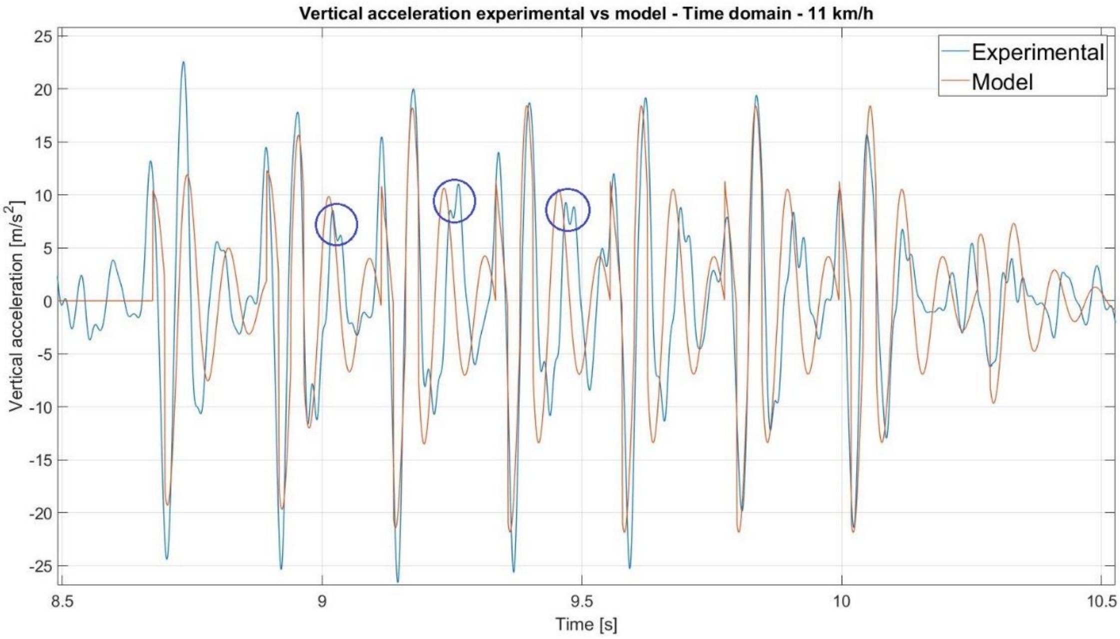

Figure 4.10 – Vertical acceleration experimental vs model in time domain at 11 km/h

In this case, it seems that by increasing the speed, the influence of the tile joints is diminished, as it can be seen that there are no longer points where the oscillation frequency doubles, but only areas, some of which are highlighted with a blue circle, where there are small disturbances. In this case too, the model seems to faithfully follow the trend of the experimental oscillations in time domain. In the frequency domain, the oscillation frequencies are also very similar, but there are differences in the amplitudes, as shown in figure 4.11.

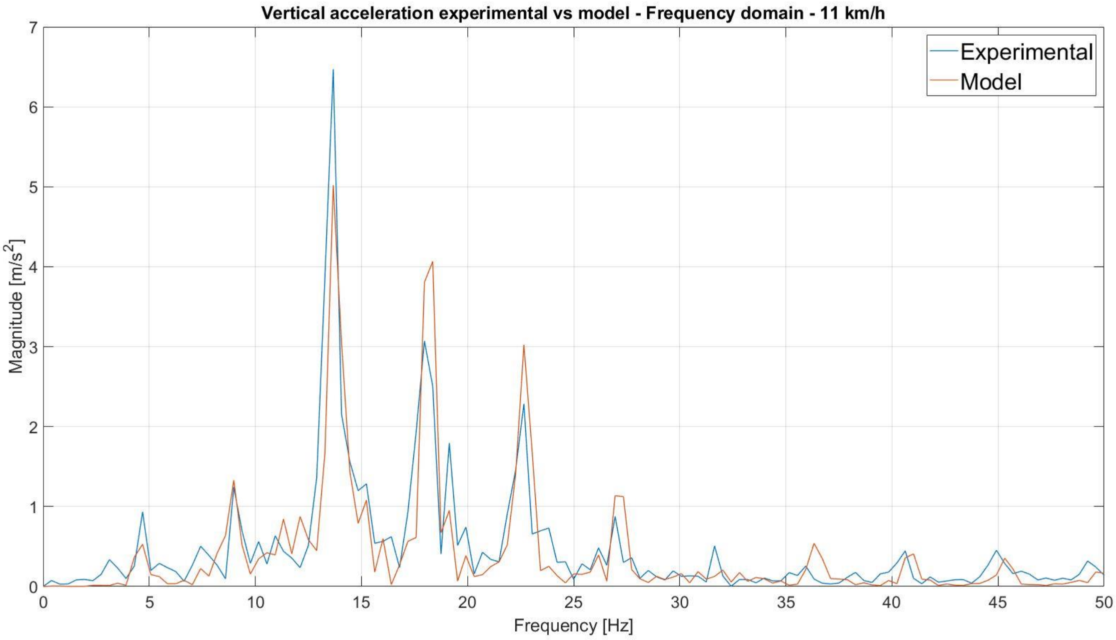

Figure 4.11 – Vertical acceleration experimental vs model in frequency domain at 11 km/h

4.3 ISO 2631 application

The ISO 2631 standard described in paragraph 1.1.1 was applied to both the experimental data and the data calculated by the model. To apply the standard, a Matlab toolbox for signal analysis called "vibrationdata" was used, which automatically applies frequency weighting and calculates the root mean square value.

After launching the program, a screen appears where it is possible to select the type of analysis to be carried out. Among the different options, there is one called "ISO Generic VC, 2631, 10816".

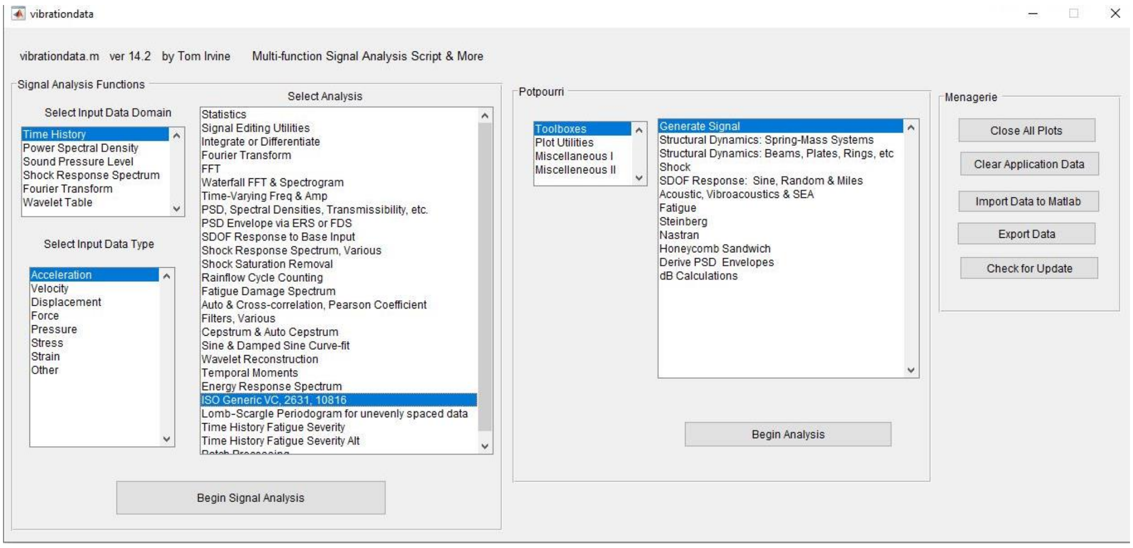

Figure 4.12 – vibrationdata toolbox interface

After selecting this analysis, a screen opens in which it is necessary to enter the data matrix to be analysed with the time in the first column and the accelerations in the second, the type of weighing to be carried out and the start and end time.

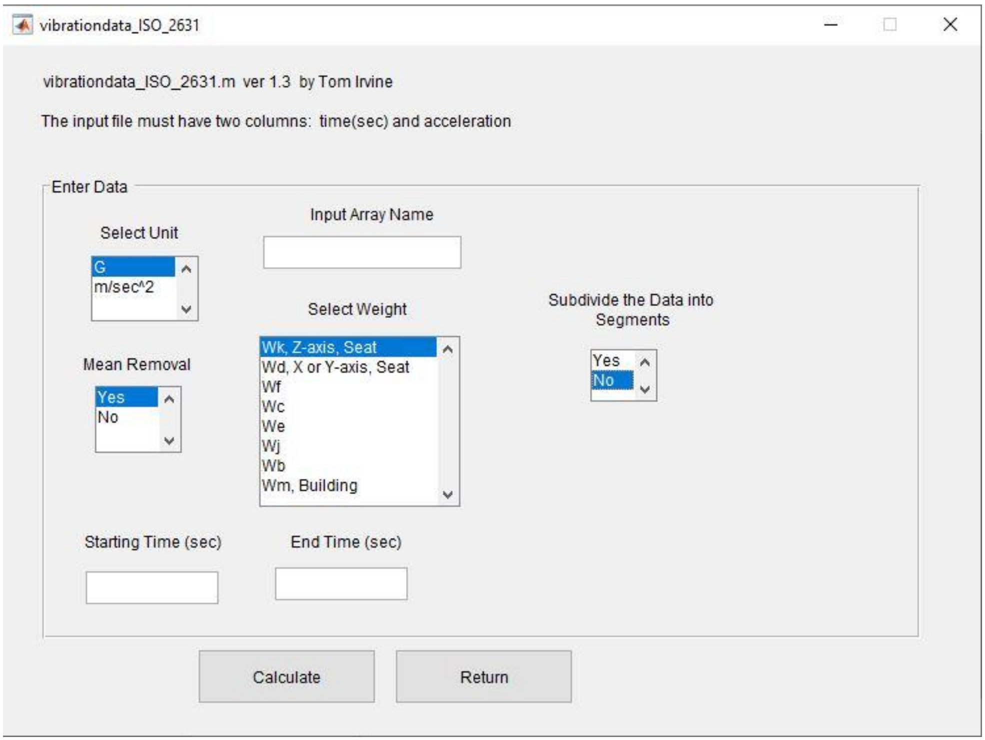

Figure 4.13 – ISO 2631 interface

By pressing the calculate button, the programme automatically applies frequency filtering and calculates the root mean square value.

This calculation was carried out on the experimental and model tests for both speeds to check that they gave compatible results with experimental data.

For the 6 km/h test, only the 4 seconds during which the vehicle passes over the speed bumps were taken:

$$\text{Experimental: } a_w = 4{,}007 \left(\frac{m}{s^2}\right) RMS$$

$$\text{Model: } a_w = 3{,}954 \left(\frac{m}{s^2}\right) RMS$$

The same thing was done on the tests at 11 km/h taking in this case only the three seconds needed for the vehicle to pass over the speed bumps:

$$\text{Experimental: } a_w = 6.343 \left(\frac{m}{s^2}\right) RMS$$

$$\text{Model: } a_w = 6.351 \left(\frac{m}{s^2}\right) RMS$$

4.4 Parameter change

After demonstrating that the behaviour of the model is very similar to what happens in reality, except for a few absolute values, it is possible to use this tool to evaluate the introduction of new components or the change of certain parameters. In this way, it is possible to understand even in an approximate way the benefit or worsening following the introduction of new parts and to make cost/benefit assessments.

4.4.1 Front suspension addition

This section evaluates the introduction of a new component on the vehicle, the front suspension. Since this part is already included in the model, it is only necessary to activate it and repeat the tests performed. It was chosen to use three suspension configurations with different stiffnesses of 200 $\frac{N}{mm}$, 160 $\frac{N}{mm}$ and 120 $\frac{N}{mm}$. It should be noted that very high stiffness values were chosen because, being a suspension with a very short stroke, it is necessary to insert a spring that not only improves the comfort of the vehicle but also avoids, in most cases, reaching the end of the stroke. The parameters kept constant are:

$$b = 50 \left(\frac{N}{m/s}\right)$$

$$stroke = 17\ mm$$

Figure 4.14 compares the accelerations measured by the steering transducer with those calculated by the model with a suspension stiffness of 200 $\frac{N}{mm}$ in the 6 $\frac{km}{h}$ test in the time domain.

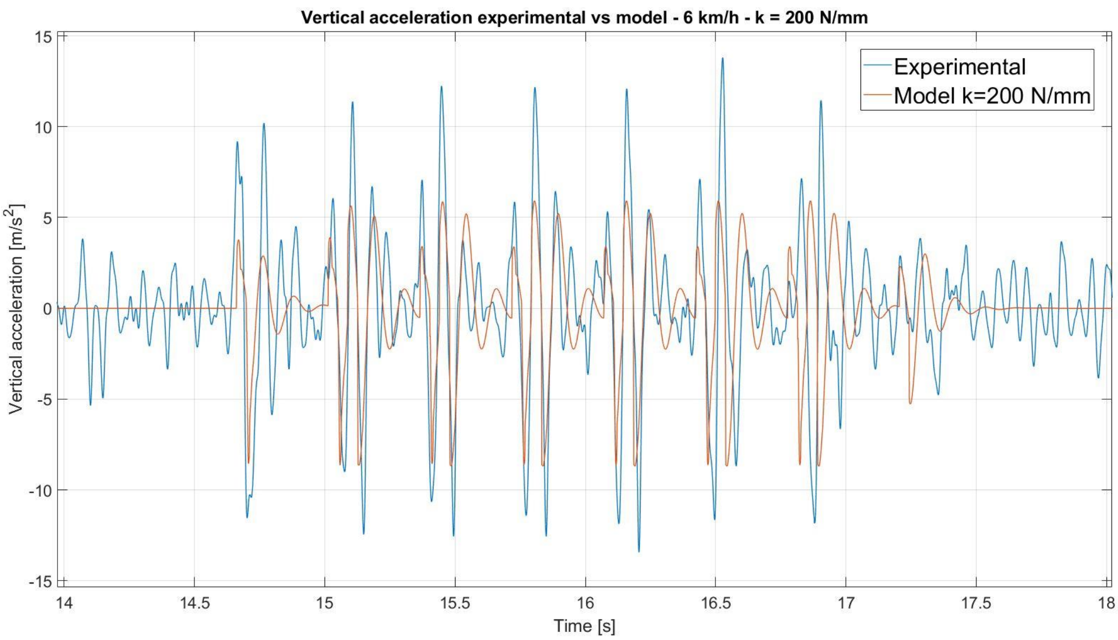

Figure 4.14 – Vertical acceleration experimental vs model - k=200 N/mm

From the graph above, it can be seen that for each step, the first two peaks due to the impact of the front wheel are lower than in the experimental data. The next graph shows the accelerations over time for the three different suspension configurations.

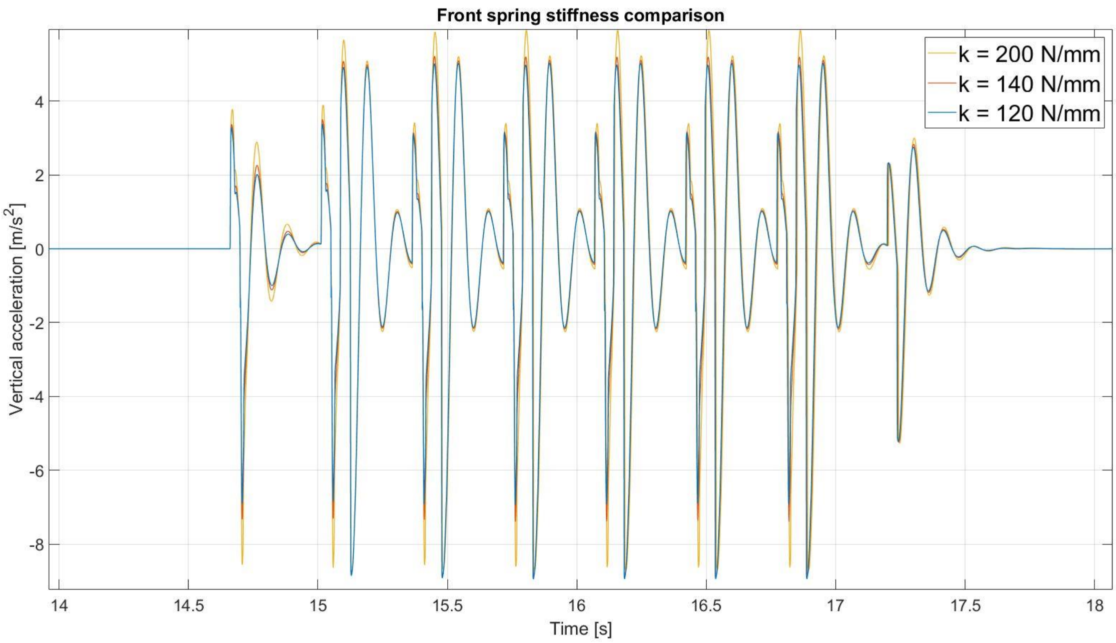

Figure 4.15 – Vertical acceleration as a function of suspension stiffness at 6 km/h

From the graph above, it can be seen that the difference between the settings lies in the absolute value of the acceleration of the first two peaks for each step, which decreases as the stiffness decreases. For each configuration, the weighted RMS accelerations were calculated using the "vibrationdata" tool, from which it emerged that as the stiffness decreases, the comfort increases, even if passing from the stiffest to the softest setting the improvement is limited.

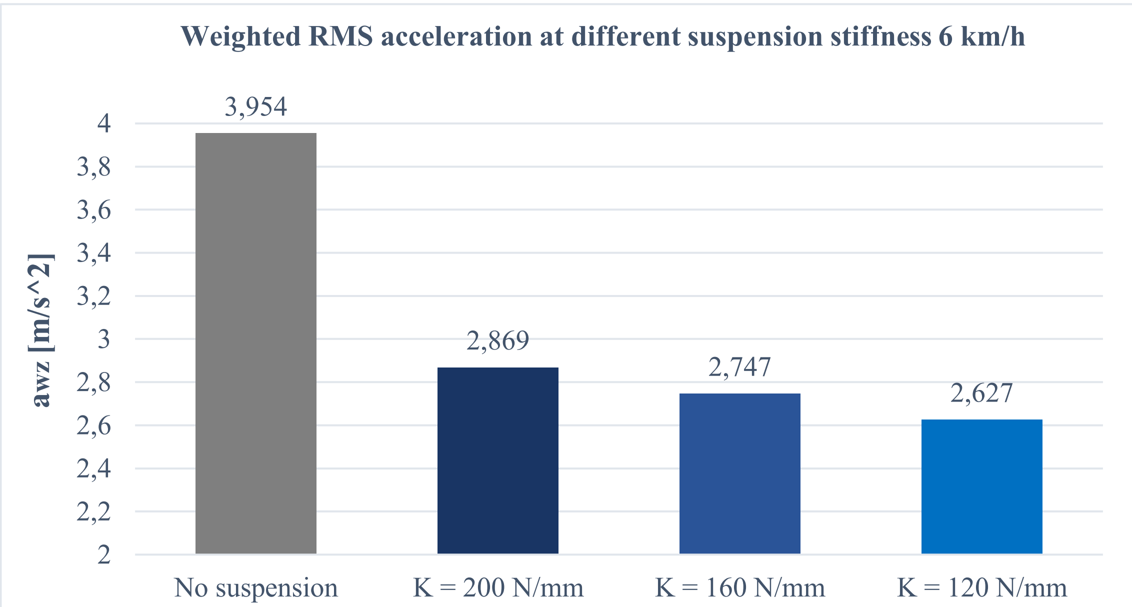

Figure 4.16 – Weighted RMS acceleration at different suspension stiffness at 6 km/h

The same operation was also carried out for the 11 km/h speed test where similar results were found, and the same considerations as above apply.

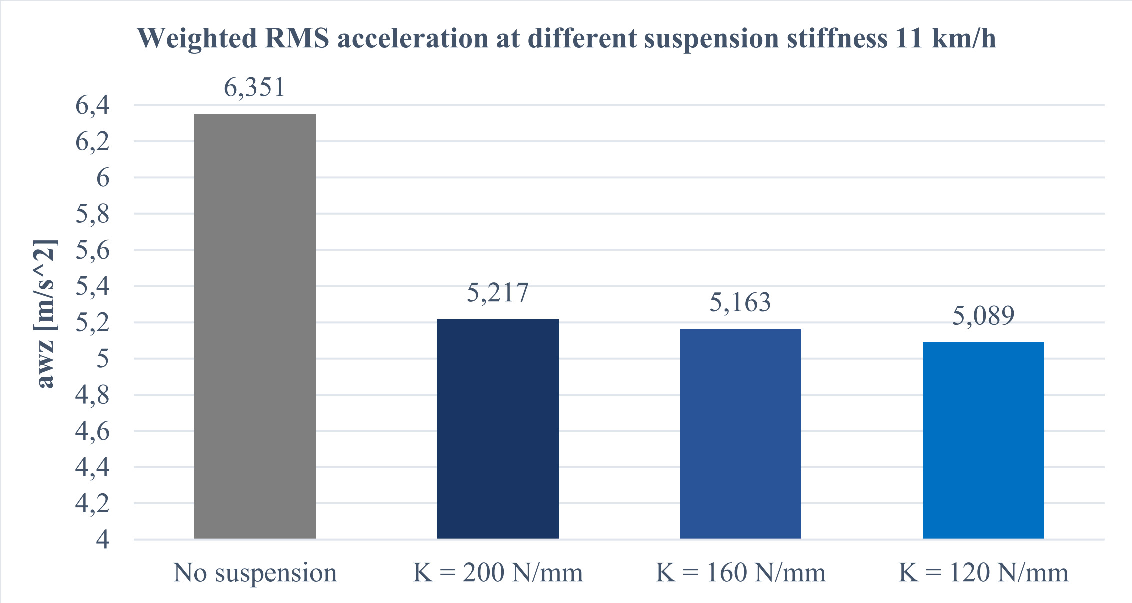

Figure 4.17 – Weighted RMS acceleration at different suspension stiffness at 11 km/h

In this case, the limiting factor that does not allow for a less rigid spring is the stroke. For the configuration with a stiffness of 120 $\frac{N}{mm}$, the static displacement with a driver weighing 80 kg is 3.1 mm, which increases to 4.4 mm if the driver's weight is assumed to be the maximum declared for this vehicle, 110 kg. This brings the effective stroke down to 12.6 mm, and since much higher obstacles than those considered in this study can be encountered when driving, it is not recommended to lower the stiffness to avoid reaching the end of the stroke.

4.4.2 Front wheel stiffness

An alternative to adding a front suspension to improve comfort is to use a softer front wheel. As in the previous paragraph, three configurations with different front wheel stiffnesses were considered: 119 $\frac{N}{mm}$, 99 $\frac{N}{mm}$ and 79 $\frac{N}{mm}$. Figure 4.18 shows the vertical acceleration trends over time in the different configurations.

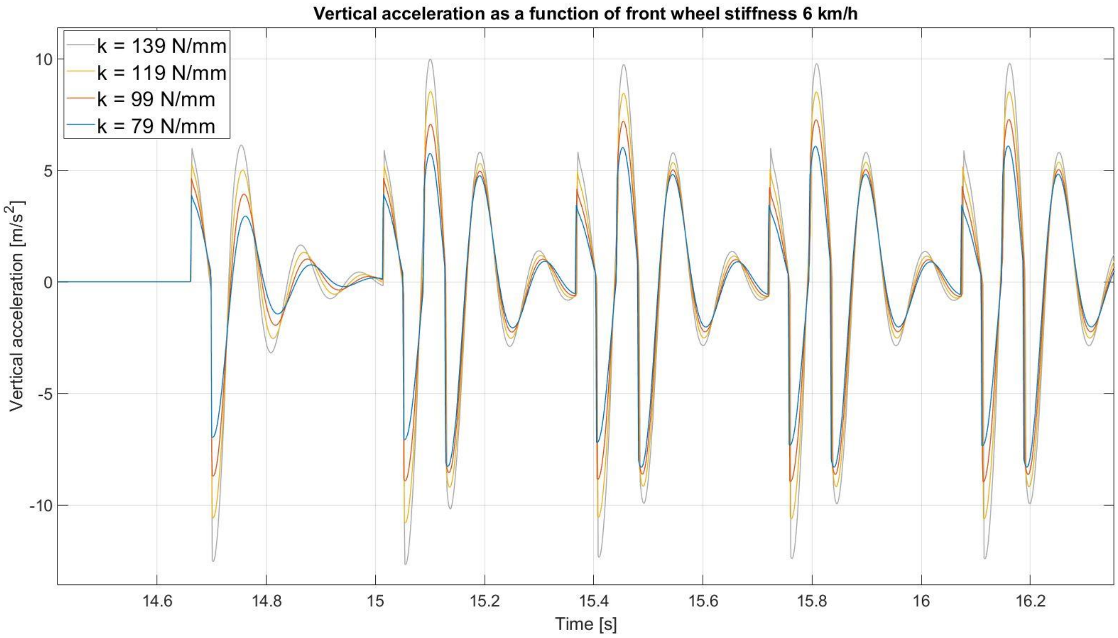

Figure 4.18 – Vertical acceleration as a function of front wheel stiffness at 6 km/h

From the above graph it can be seen that, as expected, as the stiffness of the wheel decreases, the vertical acceleration reduces. Also in this case, using the "vibrationdata" tool, the RMS weighted acceleration values were calculated, whose values are shown in figure 4.18. Comparing the results obtained in the previous paragraph, it can be seen that the sensitivity to the variation of the stiffness of the front wheel is greater than that of the suspension.

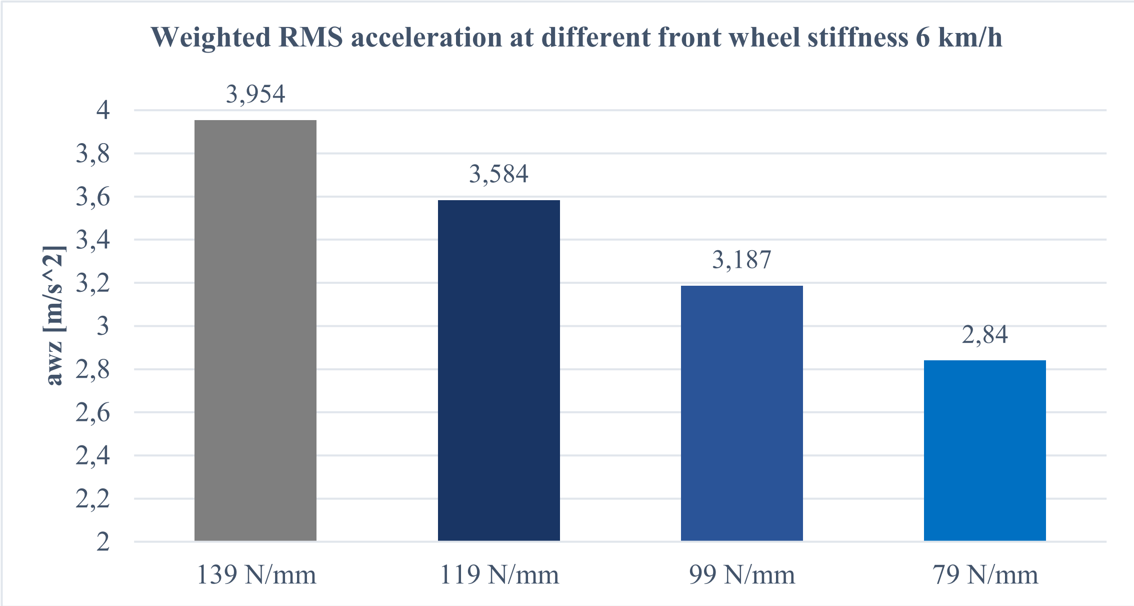

Figure 4.19 –Weighted RMS acceleration at different front wheel stiffness at 6 km/h

The same operation was also carried out for the 11 km/h speed test where similar results were found, and the same considerations as above apply.

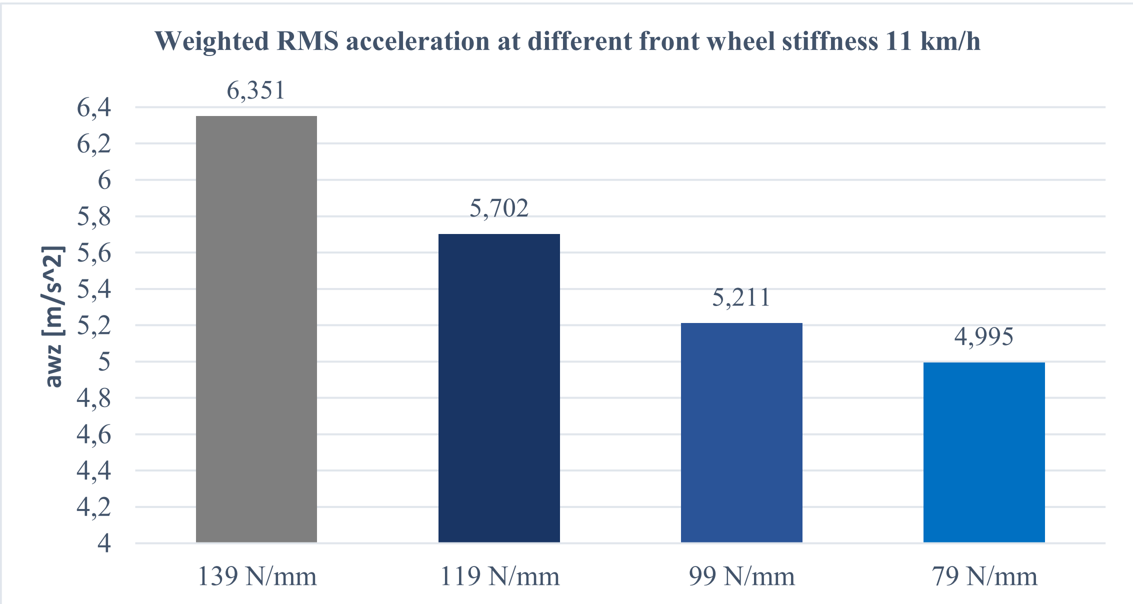

Figure 4.20 – Weighted RMS acceleration at different front wheel stiffness at 11 km/h

In this case it is necessary to check the static crush to which the front wheel is subjected. In the softest setting the static crush is 5.5 mm when the driver's weight is 80 kg and 7.4 mm when it is 110 kg. The shoulder height of the front wheel is 40 mm, so even the lower stiffness setting is a safe condition.

4.4.3 Consideration

In this paragraph, some considerations are made regarding the two solutions discussed in the previous paragraphs. With regard to the front suspension, it was found that its inclusion immediately leads to a significant decrease in the value of weighted RMS acceleration when overcoming speed bumps. The change in stiffness does not lead to a marked improvement in comfort since very stiff configurations were considered. The main limiting factor preventing the use of a less rigid spring is the short stroke. The advantages of this solution are improved comfort in shocks and the possibility of keeping the solid tyre, which is a very important feature on a vehicle of this type. On the other hand, being an additional component, its introduction leads to an increase in the cost of the vehicle.

Another way to obtain an improvement in comfort is to use a wheel with a lower vertical stiffness. In this case, it has been seen that the system is very sensitive to changes in stiffness and therefore if a good improvement is desired it is necessary to use a much softer wheel. The disadvantage of using a softer tyre is an increase in deformation leading to higher rolling resistance and increased tread wear.

Chapter 5

Conclusion

The aim of this paper was to create a dynamic model of an electric scooter on Simscape Multibody. The latter was used to try to improve the comfort of the vehicle when overcoming road obstacles. The conclusions reached are the result of an iteration aimed at matching the results obtained from the virtual simulation with the experimental data and using the same set-up to evaluate the introduction of a new component or the change of certain parameters. Despite the reduced applicability of the model due to a small number of tests and the lack of data on the wheels, virtual prototyping allows to obtain qualitative results that allow to direct the development of the vehicle towards the most appropriate choices.

However, the model described in the previous paragraphs represents a starting point for the development of an even more complete system. As explained in the paper, there are some limitations, such as the impossibility of performing steering manoeuvres. A future improvement could involve changing the modelling of the wheel to a more complex system or implementing a way of keeping the scooter balanced. It would also be possible to include components such as the electric motor and battery to perform simulations concerning energy consumption. All this presupposes the need to characterise the wheel in order to obtain reliable data and extend the applicability of the model to simulations of longitudinal and lateral dynamics.

Bibliography and sitography

- European Environment Agency - https://www.eea.europa.eu/it/themes/transport/intro
- INAIL (2019), "*La valutazione del rischio vibrazioni*" - https://www.portaleagentifisici.it/filemanager/userfiles/wbv/ValutazioneRischioVibrazioni_2019_corretto.pdf.pdf?lg=IT
- TO.TEM - https://www.totemev.com/
- Catelani D., "*La simulazione dinamica dei sistemi multi-body*" - https://home.aero.polimi.it/masarati/pe/es6/corsoadams.pdf
- Air-fom - https://air-fom.com/
- La Stampa (2019) - https://www.lastampa.it/motori/tecnologia/2019/06/08/news/michelin-uptis-primi-test-per-lo-pneumatico-del-futuro-senz-aria-e-a-prova-di-chiodo-1.36539459
- MATLAB documentation - https://it.mathworks.com/help/matlab/
- Steve Miller (2021). Simscape Vehicle Templates (https://github.com/mathworks/Simscape-Vehicle-Templates/releases/tag/21.1.2.3), GitHub. Retrieved September 29, 2021.
- MathWorks Student Competitions Team (2021). MATLAB and Simulink Racing Lounge: Vehicle Modeling with Simscape Multibody (https://www.mathworks.com/matlabcentral/fileexchange/64648-matlab-and-simulink-racing-lounge-vehicle-modeling-with-simscape-multibody), MATLAB Central File Exchange. Retrieved September 29, 2021.
- Marco Furlan (2021). MFeval (https://www.mathworks.com/matlabcentral/fileexchange/63618-mfeval), MATLAB Central File Exchange. Retrieved September 29, 2021.
- Arts Hirata (2021). Simple Suspension test (https://www.mathworks.com/matlabcentral/fileexchange/46243-simple-suspension-test), MATLAB Central File Exchange. Retrieved September 29, 2021.
- Seismic skate systems - https://seismicskate.com
- Trampa - https://trampaboards.com/trucks-c-25.html
- Stoked ride shop - https://stokedrideshop.com/blogs/trucks/the-ultimate-longboard-truck-guide
- Alvarez A., 3Dcontentcentral - https://www.3dcontentcentral.com/Download-Model.aspx?catalogid=171&id=191554

- TE connectivity - https://www.te.com/usa-en/industries/sensor-solutions/insights/condition-monitoring-white-paper.html
- Kistler - https://www.kistler.com/it/
- Fighera G., "*Meccanica delle vibrazioni*" UNICT, - http://www.diim.unict.it/users/gfichera/MSIM_file/vibrazioni_misura.pdf
- Siemens - https://www.plm.automation.siemens.com/global/it/
- Irvine T., vibrationdata toolbox - https://vibrationdata.wordpress.com/
- De Leva, P. (1996) Adjustments to Zatsiorsky-Seluyanov's Segment Inertia Parameters. Journal of Biomechanics, 29, 1223-1230. https://doi.org/10.1016/0021-9290(95)00178-6